Optimization and analysis of frequencies of multi-scale graphene/fibre reinforced nanocomposite laminates with non-uniform distributions of reinforcements

Y. Jeawon[1], G.A. Drosopoulos[1*], G. Foutsitzi[2], G.E. Stavroulakis[3], S. Adali[4]

[1]Discipline of Civil Engineering, University of KwaZulu-Natal, Durban, South Africa

[2]Department of Informatics and Telecommunications, University of Ioannina, Ioannina, Greece

[3]School of Production Engineering and Management, Technical University of Crete, Chania, Greece

[4]Discipline of Mechanical Engineering, University of KwaZulu-Natal, Durban, South Africa

* [1]Corresponding Author

Abstract

Optimal design and analysis of three-phase graphene/fibre reinforced laminated nanocomposite plates with respect to maximizing the fundamental frequency is the subject of the present study. Optimal design solutions are given for four different sets of design parameters. First design problem determines the optimal graphene contents of individual layers, the second one both graphene and fibre contents, the third optimizes the graphene and fibre contents as well as the layer thicknesses of individual layers, and the fourth problem optimizes the graphene and fibre contents, layer thicknesses and fibre orientations. Purpose of this approach is to assess and compare different levels of optimization by means of a design efficiency index and as such to determine the effectiveness of different design parameters in maximizing the fundamental frequency. Optimization is implemented using a Sequential Quadratic Programming algorithm and the mechanical properties of graphene/fibre nanocomposite are determined via micromechanical relations. Vibration analysis is conducted by the finite element method using four-noded Mindlin plate elements. Results are obtained for simply supported (SSSS), clamped (CCCC) and simply supported-clamped boundary conditions for

---

[1] Structural Engineering and Computational Mechanics Group, Discipline of Civil Engineering, University of Kwazulu-Natal, Howard College, Durban, South Africa, http://secm.ukzn.ac.za/, DrosopoulosG@ukzn.ac.za

opposite edges (SCSC). It is observed that non-uniform distributions of graphene and fibre as well as fibre orientations are quite effective in improving the design efficiency.

Keywords: Optimal design; Nano-structures; Graphene reinforcement; Vibration; Finite element analysis (FEA); Laminated nanocomposite

1. Introduction

Nanocomposite laminates are used widely in several sectors of civil, mechanical and aerospace engineering. The concept of the enhancement of traditional composite structures by utilizing advanced materials with superior mechanical properties has gained wider acceptance, implementation and applications in the last few years as noted in a number of publications [1, 2, 3]. Recent research efforts have highlighted the idea of incorporating nano-scale reinforcements, such us carbon nanotubes (CNTs) or graphene nanoplatelets (GPLs), to improve the mechanical and physical properties of polymer composites further. The specific interest in the present study is the use of GPLs as reinforcement due to their superior properties as noted in [4, 5]. Several issues concerning the reinforcement of composites by GPLs have been investigated in [6].

An important tool in the design of composite components is design optimization in order to improve their performance facilitated by the availability of several design parameters [7]. The most common way of optimizing a composite laminate is by determining the fibre orientations optimally in order to maximize (or minimize) a specific design objective. An important aspect of a design is to keep the weight of the component as low as possible. This can be achieved by placing the reinforcements mostly in the outer layers and a smaller portion of the reinforcements in the middle layers. This approach is based on the fact that reinforcements closer to the surface layers contribute more to the laminate stiffness [8]. Non-uniform fibre distribution has been implemented as a design tool in a number of studies in order to improve the design efficiency and reduce the weight [9, 10, 11]. In this case fibre volume fractions of layers become design parameters. In the present study the design parameters to maximize the fundamental frequencies include the volume fractions of graphene platelet and fibres in each layer, ply thicknesses and fibre orientations. In order to assess the effect of different design parameters on the design efficiency, the design parameters are introduced in four steps, namely, graphene content

only of each layer, graphene and fibre contents of each layer, ply thicknesses and finally fibre orientations.

Graphene is a monolayer of sp^2 hybridized carbon atoms arranged in a honeycomb structure and is well known for its exceptional mechanical properties [12]. It also possesses additional beneficial properties such as light weight, electrical conductivity and mechanical toughness [13] and presently it is being used widely in several industrial applications [14]. It was noted that Young's modulus of graphene could approach 1000 GPa and its tensile strength 130 GPa [15]. It was also noted that 0.1% GPL added to epoxy composites can increase the Young's modulus by 31% [16]. The main reason for the high reinforcing capacity of graphene is attributed to large surface area of platelets resulting in a high level load transfer from the polymer matrix to reinforcing component as observed in [17, 18]. However, the introduction of a nano-scale reinforcement into polymer matrix should also consider such effects as the diminishing returns caused by using a high amount of nano reinforcement which can lead to the nano material not dispersing in the matrix uniformly. Uniform dispersion of nano-scale reinforcements in a matrix is an important consideration as a high volume content can lead to coalescing and inadvertently affecting the stiffness and the strength of the material. Another issue is the high cost of nano materials which makes the optimal use of the nano reinforcements an important requirement to keep the material costs to a minimum. These considerations become of major importance in the design of three-phase nanocomposites (nano-scale reinforcement + fibre + matrix). Within this framework, several studies investigated the behaviour of nano-reinforced laminated structures undergoing free or forced vibrations, or subject to buckling or bending loads. One of the main areas of this research has been the study of two-phase graphene reinforced nanocomposite laminates consisting of only graphene and a matrix.

Free vibration, buckling and static bending of multi-layered and functionally graded GPL reinforced composite plates were analysed in [19]. Elastic constants of the nanocomposite were computed using the modified Halpin-Tsai micromechanical model. The results indicated that the natural frequencies and buckling loads were significantly improved with the addition of graphene. In [20], vibration damping properties of GPL reinforced NR/EPDM (Natural rubber/ethylene-propylene-diene rubber) were studied via free vibration tests. The results showed that the addition of GPLs significantly improved the damping ratio values (up to 50%) when compared to the NR/EPDM blend only.

Light weight structures are often exposed to severe vibrations and it becomes important to improve their performance by reducing the possibility of resonance. To avoid resonance, natural frequencies of the structure have to be away from the excitation frequency. One way of achieving this objective is to increase the fundamental frequency and make it higher than the excitation frequency. Another way is to increase the frequency gaps and place the excitation frequency into one of these gaps [21, 22]. The first case leads to an optimal design problem to maximize the fundamental frequency. A statistical analysis is given for the free vibrations of functionally graded graphene reinforced composite plates in [23]. The study indicates that boundary conditions and volume fractions of GPLs were the most significant parameters for the vibration response, followed by thickness ratio and distribution pattern of GPLs. More recent works on the vibration of two-phase graphene reinforced nanocomposites include [24, 25, 26, 27, 28, 29, 30, 31, 32, 33].

Recently, the research was directed towards investigating the mechanical response of three-phase multi-scale laminates. In this case, the polymer matrix is reinforced by a nano-scale material such as carbon nanotubes (CNT) or graphene as well as fibres (mostly glass or carbon) leading to a multi-scale composite involving macro (matrix), micro (fibre) and nano (CNTs or GPLs) scales. The motivation for this study emanates from the fact that the limits of improving the mechanical properties of traditional fibre reinforced composites are gradually reached [34] while the requirements for advanced material properties increase. A major reason for the high-level of reinforcement of composites by graphene platelets is the two-dimensional nature of graphene which results for the reinforcement to take place in the in-plane directions. Furthermore, graphene platelets have larger surface to volume ratios which create a larger interface for bonding [35]. In [36] it is concluded that the flexural modulus of three-phase graphene/fibre reinforced composites is 1.7, 4.5 and 6.4 times larger than those of the two-phase fibre reinforced composites, the two-phase graphene reinforced composites and the polymer host, respectively. Scanning electron microscope image analysis presented in the same article indicates that the enhancement of the mechanical properties for the three-phase composite is attributed to the synergetic effect of the fibres and the nano-reinforcement (graphene nanoplatelets) on the polymer matrix in terms of improvement of the interfacial interactions and decrease of the matrix-rich and free-volume regions. Therefore, it is expected that three-phase composites provide a further improvement over the two-phase conventional composites and two-phase nanocomposites. The advantages of a graphene

and fibre reinforcement of polymer composites have also been noted in a number of publications [36, 37, 38, 39, 40]. Studies on the bending, buckling and vibration behaviour of multi-scale three-phase laminates are given in [41, 42, 43, 44]. Numerical results of [41] indicated that the central deflection and fundamental frequencies were significantly improved by incorporating a small percentage of GPLs in a fibre-reinforced composite. In [44], it was observed that exceeding a certain fibre content in a three-phase laminate leads to a decrease in the buckling strength by reducing the volume fraction of graphene reinforced matrix.

Several studies were directed to the optimization of fibre composite laminates to improve the vibrations response [8, 45, 46, 47, 48]. However, a relatively small number of studies involved optimization of two-phase or three-phase nanocomposite laminates. In [49], vibration and optimization of CNT reinforced beam was investigated based on higher order theories. In [50], CNT and glass fibre reinforced composite plates were optimized for maximum frequency. Results indicated that higher CNT volume fraction does not necessarily increase the frequencies. It was observed that the stacking sequence can significantly influence the frequencies, especially in the case of simply supported boundary conditions.

Presently, there seems to be no work published on the optimization of the frequencies of three-phase, graphene/fibre reinforced composite laminates taking the graphene and fibre contents non-uniformly distributed across the thickness, taking the ply thicknesses non-uniform, combined with the optimal orientation of fibres. In the present study, this problem is studied in detail from analysis and optimization points of view to offer an insight on the vibration response of three-phase laminates. The main emphasis is on the optimal graphene distribution across the laminate thickness as well as on optimal graphene and fibre distributions across the thickness. In addition to these two design variables, optimizations with respect to layer thicknesses and fibre orientations are also studied in combination with optimal graphene and fibre distributions. To implement the analysis and optimization solutions for various boundary conditions, a finite element analysis code is developed based on the first-order shear deformation theory (FSDT) for the computation of the fundamental frequencies of the laminated composite. The code is then incorporated in an optimization scheme based on the sequential quadratic programming (SQP).

Section 2 of the paper presents the theoretical background for the finite element code developed to simulate the free vibration response of laminate plates. Section 3 is allocated to the micromechanical equations implemented to determine the effective material

properties of the laminate. Section 4 presents the optimization formulation and Section 5 the verification of the proposed numerical scheme by comparing the results to published research and also the ones obtained by commercial software. In Section 6, analysis results are given, investigating the effects of reinforcements of graphene and fibres on frequencies. Section 7 presents the optimal design results and Section 8 the conclusions of this work.

2. Theoretical formulation

The present study involves the vibrations of a laminated composite plate having length a in the *x*-direction, width b in the *y*-direction and with a total thickness of D as shown in Fig. 1. The plate consists of N layers with the principal material coordinates of the k^{th} lamina oriented at an angle θ_k to the laminate coordinate *x*. The *xy*−plane coincides with the mid-plane of the plate with the *z*-axis being normal to the mid-plane (Fig. 1). The vertical coordinates of the top and bottom of the k^{th} layer are given by $z = z_k$ and $z = z_{k-1}$. The polymer matrix is reinforced with graphene nanoplatelets and fibres noting that their volume fractions in each lamina could be different. Furthermore, layer thicknesses could be non-uniform and could be determined optimally.

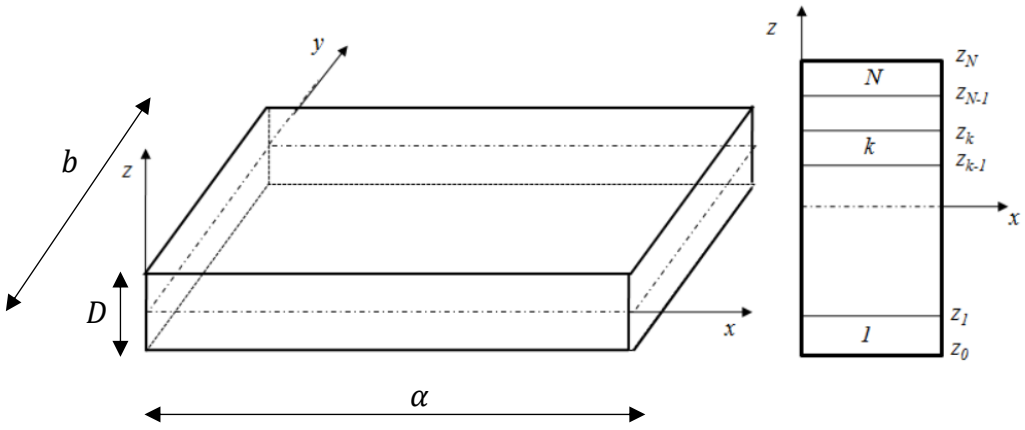

Fig 1. Geometry of the laminated plate

2.1 Mechanical displacements and strains

One of the most widely used displacement based theories for laminated plates is the first-order shear deformation theory (FSDT) which is based on the displacement field described by the equations:

$$u_1(x,y,z,t) = u(x,y,t) - z\varphi_x(x,y,t)$$
$$u_2(x,y,z,t) = v(x,y,t) - z\varphi_y(x,y,t) \quad (1)$$
$$u_3(x,y,z,t) = w(x,y,t)$$

where (u_1, u_2, u_3) are the displacements along the (x, y, z) coordinates, (u, v, w) are the displacements of a point on the mid-plane of the panel and φ_x, φ_y are the normal rotations about the x and y-axes, respectively. Using the strain–displacement relations, the bending and shear strains can be expressed as

$$\{\varepsilon_b\} = \{\varepsilon_{0b}\} + z\{\kappa\}, \qquad \{\varepsilon_s\} = \{\varepsilon_{0s}\} \quad (2)$$

where

$$\{\varepsilon_b\} = \left\{\varepsilon_{xx}, \varepsilon_{yy}, \gamma_{xy}\right\}^T, \{\varepsilon_s\} = \{\gamma_{yz}, \gamma_{xz}\}^T, \quad \{\varepsilon_{0b}\} = \left\{\frac{\partial u}{\partial x}, \frac{\partial v}{\partial y}, \frac{\partial u}{\partial y} + \frac{\partial v}{\partial x}\right\}^T \quad (3a)$$

$$\{\kappa\} = \left\{-\frac{\partial \varphi_x}{\partial x}, -\frac{\partial \varphi_y}{\partial y}, -\left(\frac{\partial \varphi_x}{\partial y} + \frac{\partial \varphi_y}{\partial x}\right)\right\}^T, \quad \{\varepsilon_{0s}\} = \left\{\frac{\partial w}{\partial y} - \varphi_y, \frac{\partial w}{\partial x} - \varphi_x\right\}^T \quad (3b)$$

2.2 Constitutive equations

For an orthotropic material possessing a plane of elastic symmetry parallel to the x-y plane, the constitutive equations for the k^{th} lamina are given by:

$$\{\sigma\}_k = [Q]_k\{\varepsilon\} \quad (4)$$

where $\{\sigma\}_k$ is the stress tensor and $\{\varepsilon\}$ is the strain tensor. $[Q]_k$ is the plane-stress reduced stiffness matrix. Bending and shear stresses for k^{th} lamina can be expressed as

$$\{\sigma_b\}_k = [Q_b]_k\{\varepsilon\}, \quad \{\sigma_s\}_k = [Q_s]_k\{\varepsilon\} \quad (5)$$

where $\{\sigma_b\}_k = \{\sigma_1, \sigma_2, \sigma_6\}^T$, $\{\sigma_s\}_k = \{\sigma_4, \sigma_5\}^T$ and

$$[Q_b]_k = \begin{bmatrix} {Q_{11}}^{(k)} & {Q_{12}}^{(k)} & 0 \\ {Q_{21}}^{(k)} & {Q_{22}}^{(k)} & 0 \\ 0 & 0 & {Q_{66}}^{(k)} \end{bmatrix} \qquad [Q_s]_k = \begin{bmatrix} {Q_{44}}^{(k)} & 0 \\ 0 & {Q_{55}}^{(k)} \end{bmatrix} \quad (6)$$

In Eqs. (6), $Q_{ij}^{(k)}$ are the plane stress-reduced stiffnesses of the k^{th} lamina [51]

$$Q_{11}^{(k)} = \frac{E_1^{(k)}}{\left(1 - v_{12}^{(k)} v_{21}^{(k)}\right)}, \quad Q_{12}^{(k)} = \frac{{v_{12}}^{(k)} E_2^{(k)}}{\left(1 - v_{12}^{(k)} v_{21}^{(k)}\right)} = Q_{21}^{(k)}, \quad Q_{22}^{(k)} = \frac{E_2^{(k)}}{(1 - v_{12}^{(k)} v_{21}^{(k)})},$$

$$Q_{66}^{(k)} = G_{12}^{(k)}, \qquad Q_{44}^{(k)} = k_s G_{23}^{(k)}, \qquad Q_{55}^{(k)} = k_s G_{13}^{(k)}$$

where $E_1^{(k)}$, $E_2^{(k)}$ are the longitudinal and transverse moduli, $v_{12}^{(k)}$, $v_{21}^{(k)}$ are the Poisson's ratios, $G_{12}^{(k)}$, $G_{23}^{(k)}$, $G_{13}^{(k)}$ are the shear moduli of the k^{th} layer and k_s is a shear correction factor taken as $\frac{5}{6}$. The reduced stiffness $Q_{ij}^{(k)}$ of the k^{th} lamina can be transformed to $\bar{Q}_{ij}^{(k)}$ as

$$\left[\overline{Q}\right]_{(k)} = \left([L]^T [Q][L]\right)_{(k)} \tag{7}$$

where [*L*] is a transformation matrix for the fibre angle θ_k of the k^{th} lamina [51].

2.3 Finite element formulation and eigenvalue problem

In the present study, the laminated plate has been discretized using a four-noded isoparametric quadrilateral Lagrangian element with five degrees of freedom (DOF) per node. The generalized displacement vector is interpolated as:

$$\{\overline{u}(x,y,t)\} \equiv \left\{u, v, w, \varphi_x, \varphi_y\right\}^T = [N_u]\{d\}_e = \sum_{j=1}^{4} \left(N_j [I]_{5x5} \left\{d_j\right\}_e\right) \tag{8}$$

where $\left\{d_j\right\}_e = \left\{u_j, v_j, w_j, \varphi_{xj}, \varphi_{yj}\right\}^T$ corresponds to the j^{th} node of the element and N_j are the shape functions. Substituting Eq. (8) into Eqs. (2) gives

$$\{\overline{\varepsilon}(x,y,t)\} = [B]\{d\}_e = \sum_{j=1}^{4} \left([B_j]\left\{d_j\right\}_e\right) \tag{9}$$

or equivalently

$$\{\overline{\varepsilon}\} = \begin{Bmatrix} \{\varepsilon_{b0}\} \\ \{\kappa\} \\ \{\varepsilon_{s0}\} \end{Bmatrix} = \begin{bmatrix} [B_b] \\ [B_k] \\ [B_s] \end{bmatrix} \{d\}_e = \sum_{j=1}^{4} \left(\begin{bmatrix} [B_b]_j \\ [B_k]_j \\ [B_s]_j \end{bmatrix} \left\{d_j\right\}_e \right) \tag{10}$$

where

$$\left[B_b\right]_j = \begin{bmatrix} \partial_x & 0 & 0 & 0 & 0 \\ 0 & \partial_y & 0 & 0 & 0 \\ \partial_y & \partial_x & 0 & 0 & 0 \end{bmatrix} N_j, \quad \left[B_k\right]_j = \begin{bmatrix} 0 & 0 & 0 & -\partial_x & 0 \\ 0 & 0 & 0 & 0 & -\partial_y \\ 0 & 0 & 0 & -\partial_y & -\partial_x \end{bmatrix} N_j, \quad \left[B_s\right]_j = \begin{bmatrix} 0 & 0 & \partial_x & -1 & 0 \\ 0 & 0 & \partial_y & 0 & -1 \end{bmatrix} N_j$$

and $\partial_x = \partial / \partial x$, $\partial_y = \partial / \partial y$.

Using Hamilton's principle, the governing equation of the laminated plate subject to mechanical loads is expressed as

$$\int_0^{t0}(\delta T - \delta U + \delta W)\, dt = 0 \tag{11}$$

where *U* is the strain energy, *T* is the kinetic energy and *W* is the work done by the mechanical forces of the laminated composite plate. Analytic expressions of *U*, *T* and *W* are given in the Appendix.

The global form of the final governing equation is then expressed as

$$[M]\{\ddot{d}\} + [K]\{d\} = \{F_m\} \tag{12}$$

where [*M*], [*K*], {*d*} and $\{F_m\}$ are global mass matrix, global linear stiffness matrix, global displacement and force vectors, respectively. The generalized governing Eq. (12) can be employed to study the free vibration by dropping the force term as:

$$[K]\{d\} = \lambda[M]\{d\} \tag{13}$$

with the eigenvalue $\lambda = \omega^2$ where ω is the frequency of natural vibrations. Eq. (13) is solved within the framework of the finite element method using Cholesky factorization [52]. This method can be adopted since the stiffness matrix [*K*] is symmetric and the mass matrix [*M*] is symmetric positive-definite. The solution of the eigenvalue problem is implemented within MATLAB [53, 54].

3. Effective material properties using micromechanics equations

The laminate under consideration is a three-phase graphene and fibre reinforced polymer nanocomposite. The concept of the three-phase material relies on the need to enhance its structural response by adding a small quantity of nano-reinforcement (graphene nanoplatelets in the present study), and improving its mechanical properties by doing so. First, particles of the nano-reinforcement are distributed into the matrix, resulting in a nano-reinforced, isotropic matrix. Then, the nano-reinforced matrix is further reinforced with fibres.

The effective material properties of the nano-reinforced matrix are derived in this article using the Halpin-Tsai model and the rule of mixtures. This micromechanical homogenization approach is widely adopted in published research to capture the effective response of graphene reinforced laminates, see for example [55, 56, 57, 58].

For the calculation of the effective properties of the three-phase fibre/graphene reinforced matrix, a second set of micromechanics equations is adopted in this article. This set of equations is traditionally used to derive the effective material properties of a fibre reinforced matrix involving two-phase fibre reinforced composites [11]. This concept of using micromechanical homogenization schemes for three-phase laminates, initially adopted for two-phase fibre reinforced composites, has been elaborated in several publications. For instance, micromechanics equations adopted in [59] for a two-phase fibre reinforced composite, are also used in [41] to derive the effective material properties of three-phase fibre/graphene reinforced matrix. The same concept of using micromechanics approaches for three-phase composites, which had initially been adopted for two-phase composites, has also been implemented in a number of publications involving three-phase CNT/fibre reinforced laminates [42, 50].

Elastic constants in this article are computed from the applicable micromechanical equations. First, the effective material properties of the graphene reinforced matrix are computed using the micromechanical equations applicable to uniformly distributed GPLs. Next step involves the computation of the material properties of the three-phase graphene/fibre reinforced composite using the applicable micromechanics equations.

3.1 Graphene reinforced matrix

In this section, Young's and shear moduli, Poisson's ratio and density of graphene reinforced matrix are computed using the micromechanical equations presented in [55, 60, 61, 62]. In the equations, subscripts *GPL*, *M* and *GM* denote graphene nanoplatelets (*GPL*), the matrix (*M*) and the graphene reinforced matrix (*GM*). Young's modulus of the GPLs reinforced matrix is given by

$$E_{GM} = \left(\frac{3}{8}\frac{1+\xi_L \eta_L V_{GPL}}{1-\eta_L V_{GPL}} + \frac{5}{8}\frac{1+\xi_w \eta_w V_{GPL}}{1-\eta_w V_{GPL}}\right) \times E_M \tag{14}$$

where V_{GPL} denotes the volume content of GPLs. Parameters ξ_L and ξ_w are given in Eq. (15) in terms of the length (l_{GPL}), the width (w_{GPL}) and the thickness (h_{GPL}) of GPLs:

$$\xi_L = 2\frac{l_{GPL}}{h_{GPL}}, \qquad \xi_w = 2\frac{w_{GPL}}{h_{GPL}} \tag{15}$$

Symbols η_L and η_w in Eq. (14) are calculated next in terms of Young's moduli E_{GPL} of the graphene nanoplatelets and E_M of the matrix as

$$\eta_L = \frac{(E_{GPL}/E_M)-1}{(E_{GPL}/E_M)+\xi_L} \quad , \qquad \eta_w = \frac{(E_{GPL}/E_M)-1}{(E_{GPL}/E_M)+\xi_w} \tag{16}$$

The volume content of graphene nanoplatelets can be computed in terms of its weight fraction W_{GPL} as

$$V_{GPL} = \frac{W_{GPL}}{W_{GPL}+(\rho_{GPL}/\rho_M)(1-W_{GPL})} \tag{17}$$

where ρ_{GPL} and ρ_M represent the mass densities of graphene nanoplatelets and the polymer matrix, respectively. Poisson's ratio, shear modulus and the density of the graphene reinforced matrix are given by

$$v_{GM} = v_{GPL}V_{GPL} + v_M(1 - V_{GPL}) \tag{18}$$

$$G_{GM} = \frac{E_{GM}}{2(1+v_{GM})} \tag{19}$$

$$\rho_{GM} = \rho_{GPL}V_{GPL} + \rho_M(1 - V_{GPL}) \tag{20}$$

3.2 Graphene and fibre reinforced matrix

Fibre reinforcement of the graphene reinforced matrix improves the properties of the composite further. The fibres employed for this purpose are unidirectional and continuous. Young's moduli, shear modulus, Poisson's ratio and density of the graphene/fibre reinforced nanocomposite are computed via micromechanical relations given in [11]:

$$E_{11} = E_{F11}V_F + E_{GM}(1 - V_F) \tag{21}$$

$$E_{22} = E_{GM}\left(\frac{E_{F22}+E_{GM}+(E_{F22}-E_{GM})V_F}{E_{F22}+E_{GM}-(E_{F22}-E_{GM})V_F}\right) \tag{22}$$

$$G_{12} = G_{13} = G_{GM}\left(\frac{G_{F12}+G_{GM}+(G_{F12}-G_{GM})V_F}{G_{F12}+G_{GM}-(G_{F12}-G_{GM})V_F}\right) \tag{23}$$

$$G_{23} = \frac{E_{22}}{2(1+v_{23})} \tag{24}$$

$$v_{12} = v_{F12}V_F + v_{GM}(1 - V_F) \tag{25}$$

$$v_{23} = v_{F12}V_F + v_{GM}(1 - V_F)\left(\frac{1+v_{GM}+v_{12}E_{GM}/E_{11}}{1-v_{GM}^2 + v_{12}v_{GM}E_{GM}/E_{11}}\right) \quad (26)$$

$$\rho = \rho_F V_F + \rho_{GM}(1 - V_F) \quad (27)$$

Subscripts *GM* and *F* refer to graphene reinforced matrix and fibres, respectively. The fibre volume content is represented by V_F and the density of fibres by ρ_F.

4. Optimal design problem

The design objective is the maximization of the fundamental frequency under different boundary conditions and employing a number of design parameters. Design parameters include the distributions of GPLs and fibres across the thickness, layer thicknesses and the fibre orientations. The constraints imposed on the optimization include the total weight of GPLs, total volume content of fibres as well as the weight content of GPLs and the volume content of fibres in individual layers.

The first two optimization problems involve laminates with uniform layer thicknesses with the distributions of GPLs (Problem 1) and GPLs plus fibres (Problem 2) taken as non-uniform across the thickness and their distributions across the thickness are to be determined optimally. The next optimization problem involves laminates with non-uniform layer thicknesses in addition to having non-uniform distributions of GPLs and fibres (Problem 3). In the final optimization problem (Problem 4), the fibre orientations are also specified as design variables in addition to the previous three design variables. As such Problem 4 has four design variables, namely, GPL and fibre distributions, layer thicknesses and fibre orientations.

Dimensions of the composite laminate are given by a in the *x*-direction and b in the *y*-direction as shown in Fig. 1. The total laminate thickness is D and the number of layers is *N.* In the first two optimization problems, thickness of each layer is specified as constant and equal to h with $Nh = D$. In the third and fourth optimization problems, the thicknesses h_i of layers are taken as design variables leading to laminates with non-uniform layer thicknesses with $\sum_{i=1}^{N} h_i = D$. The fibre and graphene volume contents of each layer are denoted as V_{Fi} and V_{GPLi}, respectively.

4.1 Formulation for laminates with uniform layer thicknesses (Problems 1 and 2)

The volume of fibres in each layer is given by $Vol_{Fi} = abhV_{Fi}$ and the total volume of fibres in the laminate by $Vol_{FT} = \sum_{i=1}^{N} Vol_{Fi} = abh\sum_{i=1}^{N} V_{Fi}$ for a laminate with *N* layers. The volume of the laminated plate is given by $Vol_{plate} = abD$. The maximum amount (volume) of fibres available for the laminate is specified as $Vol_{F\max} = abDV_{F\max}$ where $V_{F\max}$ is the maximum fibre volume content of the laminate. Based on these definitions, the design constraints for the total fibre volume are given by

$$Vol_{FT} \le Vol_{F\max} \Rightarrow abh\sum_{i=1}^{N} V_{Fi} \le abDV_{F\max} \Rightarrow \frac{h}{D}\sum_{i=1}^{N} V_{Fi} \le V_{F\max} \tag{28}$$

In the specific case of a composite laminate with 8 layers which is studied in the numerical results sections, Eq. (28) becomes:

$$\frac{h}{8h}\sum_{i=1}^{8} V_{Fi} \le V_{F\max} \Rightarrow \frac{1}{8}\sum_{i=1}^{8} V_{Fi} \le V_{F\max} \tag{29}$$

A similar formulation is adopted for the constraint on the overall weight of graphene nanoplatelets and for an 8-layered laminate, the constraint is given as

$$\frac{1}{8}\sum_{i=1}^{8} W_{GPLi} \le W_{GPL\max} \tag{30}$$

In Eq. (30), W and W_{GPLmax} denote the weight of graphene nanoplatelets for the i^{th} layer and the maximum graphene weight for the laminate, respectively. With the design constraints defined as above, the optimization problem for an 8-layered laminate can be stated as follows:

$$\max Fundamental\ Frequency\ f(V_F, W_{GPL}, \theta) = \omega \tag{31a}$$

$$subject\ to \quad \frac{1}{8}\sum_{i=1}^{8} V_{Fi} \le V_{F\max} \tag{31b}$$

$$\frac{1}{8}\sum_{i=1}^{8} W_{GPLi} \le W_{GPL\max} \tag{31c}$$

$$W_{GPLi} \ge 0 \tag{31d}$$

$$d_1 \le V_{Fi} \le d_2 \tag{31e}$$

$$-90^o \le Fibre\ angle\ \theta\ \le 90^o \tag{31f}$$

Eq. (31d) states that graphene weight of each layer must be greater than or equal to zero and Eq. (31e) imposes lower and upper limits d_1 and d_2 on the fibre volume content for each layer. As shown in Eqs. (31), each layer represents a three-phase material since the contents of graphene and fibre reinforcement are greater than zero. If for a layer, the case of zero graphene content arises (case of equality in Eq. (31d)), then the composite becomes two-phase. However, this is determined by the optimization algorithm since the code is set up for three-phase composites. Practically, some zero graphene layers arise in the middle of the laminate as observed in the results sections.

In order to assess the effectiveness of an optimal design, that is, the increase in the fundamental frequency as compared to a benchmark, a design efficiency factor is introduced. It is defined as the ratio of the maximum fundamental frequency ω_{max} of the optimally designed laminate and a reference frequency ω_0. The reference frequency corresponds to a laminate with uniformly distributed graphene and fibres across the thickness of the laminate with the efficiency factor for an 8-layered laminate defined as

$$\eta = \frac{\omega_{\max}(V_F, W_{GPL}, \theta)}{\omega_0(V_i = \frac{V_{f\max}}{8}, W_{GPLi} = \frac{W_{GPL\max}}{8}, i = 1,2,,...,8)} \tag{32}$$

4.2 Formulation for non-uniform layer thicknesses (Problems 3 and 4)

For a laminate with non-uniform layer thicknesses, i.e., each layer having a different thickness, the layer thicknesses h_i become design variables to be determined optimally subject to the total thickness constraint $\sum_{i=1}^{N} \frac{h_i}{D} = 1$. The volume of fibres in each layer is given by $Vol_{Fi} = abh_iV_{Fi}$ and the total volume of fibres in the laminate by $Vol_{FT} = \sum_{i=1}^{N} Vol_{Fi} = ab\sum_{i=1}^{N} h_iV_{Fi}$ for a laminate with N layers. Design constraint on the total fibre volume content Vol_{FT} is given by

$$Vol_{FT} \le Vol_{F\max} \Rightarrow ab\sum_{i=1}^{N} h_iV_{Fi} \le abDV_{F\max} \Rightarrow \frac{1}{D}\sum_{i=1}^{N} h_iV_{Fi} \le V_{F\max} \tag{33}$$

A similar constraint applies to the total weight of graphene platelets and is given by

$$\frac{1}{D}\sum_{i=1}^{N} h_i W_{GPLi} \le W_{GPL\max} \tag{34}$$

In the numerical results sections, optimization of an 8-layered laminate is studied. For this specific case, the optimal design problem can be stated as follows:

$$\max \text{fundamental frequency } f\left(V_F, W_{GPL}, \frac{h_i}{D}, \theta i\right) = \omega \tag{35a}$$

$$\text{subject to} \qquad \frac{1}{D}\sum_{i=1}^{8} h_i V_{Fi} \le V_{F\max} \tag{35b}$$

$$\frac{1}{D}\sum_{i=1}^{8} h_i W_{GPLi} \le W_{GPL\max} \tag{35c}$$

$$W_{GPL} \ge 0 \tag{35d}$$

$$d_1 \le V_F \le d_2 \tag{35e}$$

$$-90^o \le \text{Fibre angles } \theta i \le 90^o \tag{35f}$$

For this case, the design efficiency factor is defined as

$$\eta = \frac{\omega_{\max}(V_F, W_{GPL}, \frac{hi}{D}, \theta)}{\omega_0(V_i = \frac{V_{f\max}}{8}, W_{GPLi} = \frac{W_{GPL\max}}{8}, h_i = \frac{D}{8}, i = 1,2,,...,8)} \tag{36}$$

where the denominator corresponds to a laminate with uniform graphene and fibre distributions as well as having uniform layer thicknesses.

4.3 Solution of the optimization problem

Numerical solutions of the optimization problems are obtained by a Sequential Quadratic Programming algorithm (SQP). This is an effective optimization method which generates steps by solving quadratic sub-problems for nonlinearly constrained problems [63, 64, 65]. In particular, an approximation of the Hessian of the Lagrangian function is considered at each major iteration using a quasi-Newton updating method. This is then used to generate a Quadratic Programming sub-problem the solution of which is used to define a search direction. This scheme is briefly presented below. The optimization problem with nonlinear equality and inequality constraints is given by [63]:

$$\begin{gathered} \min f(x) \\ subject\ to\ c_i(x) = 0, i \in E \\ c_i(x) \geq 0, i \in I \end{gathered} \tag{37}$$

The problem is then linearized into:

$$\min_p f_k + \nabla f_k^T p + \frac{1}{2} p^T \nabla_{xx}^2 L_k p$$

$$subject\ to\ \nabla c_i(x_k)^T p + c_i(x_k) = 0, i \in E \tag{38}$$

$$\nabla c_i(x_k)^T p + c_i(x_k) \geq 0, i \in I$$

The solution of the problem formulated above is implemented within MATLAB [53,54]. It is noted that since the MATLAB algorithms mentioned above are originally defined for minimization, the objective functions presented in Eqs. (31) and (35) are modified as follows:

$$\min Fundamental\ Frequency\ f(V_F, W_{GPL}, \theta) = -\omega.$$

The fundamental frequency is calculated by solving the eigenvalue problem. This solution is implemented within the optimization algorithm aiming to maximize the fundamental frequency as defined in the optimization formulation, considering the constraints presented in sections 4.1 and 4.2. In particular, the finite element model for the composite laminate is included in the optimization algorithm. The classical steps of the finite element method are implemented, the mass and the stiffness of the structure are determined and the eigenvalue problem is solved, resulting in the computation of the fundamental eigenfrequency. Then, optimization is implemented until the optimal solution satisfying the constraints is obtained.

5. Verification of the numerical approach

In the numerical results sections, the non-dimensional form of the fundamental frequency ω, namely, Ω is used which is given by

$$\Omega = \omega D \sqrt{\frac{\rho_M}{E_M}} \tag{39}$$

Verification of the method of solution implemented in the present study is done by comparing the present results with the results available in the literature and also with the results obtained by using a commercial software package. In the computations, the

material properties given in Table 1 are used. For the dimensions of the GPLs, the following values are used: l_{GPL} = 2.5 μm, w_{GPL} = 1.5 μm, h_{GPL} = 1.5nm. The graphene weight content is specified as $W_{GPL} = 1\%$. First, the natural frequencies obtained by the present method are compared in Table 2 with the results available in the literature, for the case of a GPL reinforced laminate. Results are given using the non-dimensionalized frequency defined in Eq. (39). The same non-dimensional frequency is used for numerical results presented in this work. Comparisons are given for the case of an isotropic plate (zero graphene and fibre content), as well as for the case of a graphene reinforced plate (with zero fibre content). As shown in Table 2, for both cases, a close agreement between the published research and the present model is observed.

Table 1: Material properties of GPLs, matrix, carbon and glass fibres

Material	E_{11}**(GPa)**	E_{22} **(GPa)**	G_{12} **(GPa)**	v_{12}	**Density (kg/m^3)**
GPL	1010	1010	$E_{11}/(2(1+v))$	0.186	1060
Matrix	3	3	$E_{11}/(2(1+v))$	0.34	1200
Carbon fibres	263	19	27.60	0.20	1750
Glass fibres	72.4	72.4	$E_{11}/(2(1+v))$	0.20	2400

Table 2: Comparison of non-dimensional frequencies Ω of simply supported (SSSS) square plates reinforced by GPLs with the thickness/length ratio of $D/a = 0.1$

Pattern	Method	Mode	
		1	2
Isotropic plate (zero graphene and fibre content)	Present/Mesh 5x5	0.0610	0.1611
	Present/Mesh 10x10	0.0590	0.1441
	Present/Mesh 15x15	0.0587	0.1413
	Ref. [66]	0.0584	0.1391
	Ref. [27]	0.0584	0.1390
Uniformly distributed GPLs with W_{GPL}=1%	Present/Mesh 5x5	0.1267	0.3352
	Present/Mesh 10x10	0.1228	0.2999
	Present/Mesh 15x15	0.1221	0.2941
	Ref. [66]	0.1216	0.2895
	Ref. [27]	0.1216	0.2895

Frequencies of the same composite laminate have been computed using ABAQUS commercial finite element analysis package and compared with the results obtained by the present method of solution. Four node shell elements and a 10x10 mesh have been used in the ABAQUS implementation. Then, several cases were examined as shown in Table 3 involving laminates with different number of layers and fibre angles as well as different boundary conditions. In all these cases, glass fibres are used as reinforcement with fibre content set to 50% for each layer. Results indicate a good agreement between the natural frequencies obtained by the model developed in this article and using the commercial software.

Table 3: Comparison of non-dimensionalized frequencies Ω of GPLs/glass fibre square plate with thickness/length ratio of $D/a = 0.1$, $W_{GPL} = 1\%$ and fibre volume content is 50%

Boundary conditions	**Pattern**	**Stacking sequence**	**Method**	**Mode**	
				1	**2**
SSSS	1 layer	[45]	Present	0.1579	0.3647
			Commercial software	0.1555	0.3601
	3 layers	[0/90/0]	Present	0.1500	0.3498
			Commercial software	0.1483	0.3454
	8 layers	$[0/30/45/90]_s$	Present	0.1530	0.3565
			Commercial software	0.1511	0.3520
CCCC	8 layers	$[0/30/45/90]_s$	Present	0.2639	0.4937
			Commercial software	0.2611	0.4885
SCSC	8 layers	$[0/30/45/90]_s$	Present	0.2226	0.3891
			Commercial software	0.2204	0.3844

For further validation of the proposed model, the optimal fundamental frequency obtained by the proposed approach is compared with a number of discrete simulations conducted using the commercial software package. A two-layer hybrid laminate finite element model is developed and several simulations are conducted, adopting different stacking sequences. As shown in Table 4, both the proposed approach and the commercial software result in the same optimal stacking sequences as well as giving a very close value for the optimal fundamental frequency.

Table 4: Comparison of non-dimensional frequencies Ω with those obtained from the commercial software package for a GPLs/glass fibre SSSS square plate with thickness/length ratio $D/a = 0.1,\ W_{GPL} = 1\%$ and fibre volume content 50%

Commercial software discrete simulations			**Proposed optimization code**	
Case	Stacking sequence	Non-dimensionalized frequency	Optimal stacking sequence	Optimal non-dimensionalized frequency
1	[0/0]	0.1483	[**45/45**]	**0.1579**
2	[30/0]	0.1505		
3	[45/0]	0.1510		
4	[60/0]	0.1496		
5	[90/0]	0.1464		
6	[0/30]	0.1505		
7	[30/30]	0.1537		
8	[45/30]	0.1543		
9	[60/30]	0.1528		
10	[90/30]	0.1496		
11	[0/45]	0.1510		
12	[30/45]	0.1543		
13	[**45/45**]	**0.1555**		
14	[60/45]	0.1543		
15	[90/45]	0.1510		
16	[0/60]	0.1496		
17	[30/60]	0.1528		
18	[45/60]	0.1543		
19	[60/60]	0.1537		
20	[90/60]	0.1505		
21	[0/90]	0.1464		
22	[30/90]	0.1496		
23	[45/90]	0.1510		
24	[60/90]	0.1505		
25	[90/90]	0.1483		

6. Analysis of the effects of reinforcements on frequencies

Before presenting the results for the optimal design problems, some preliminary simulations are conducted with the GPLs and fibres distributed uniformly across the layers, i.e., all layers having the same volume content of the reinforcements. The objective of this exercise is to assess the effect of different graphene and/or fibre contents on the fundamental frequency and to study the trends as reinforcements increase. This study is conducted to observe the behaviour of three-phase composites which may have some unusual trends in terms of the effect of different reinforcements on frequencies. For this purpose, uniform glass or carbon fibre contents of 30% or 60% are specified for each layer. The results of this exercise are shown in Figs. 2 and 3 for different boundary conditions. In Fig. 2 results for an anti-symmetric stacking sequence and in Fig. 3 for a symmetric stacking sequence are given.

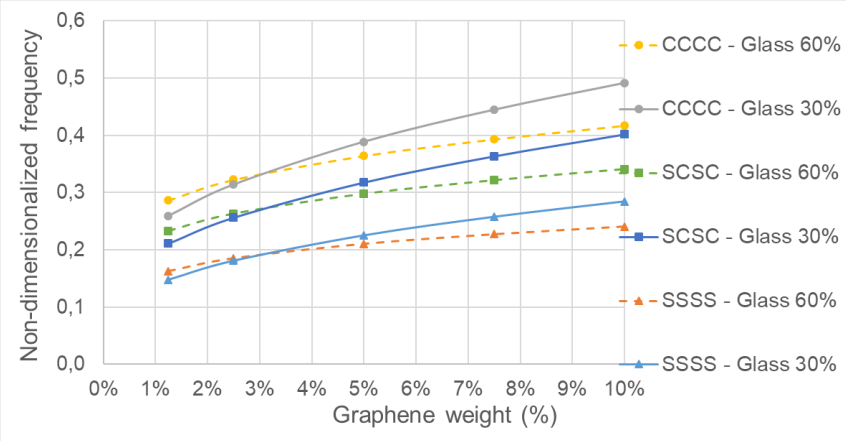

(a)

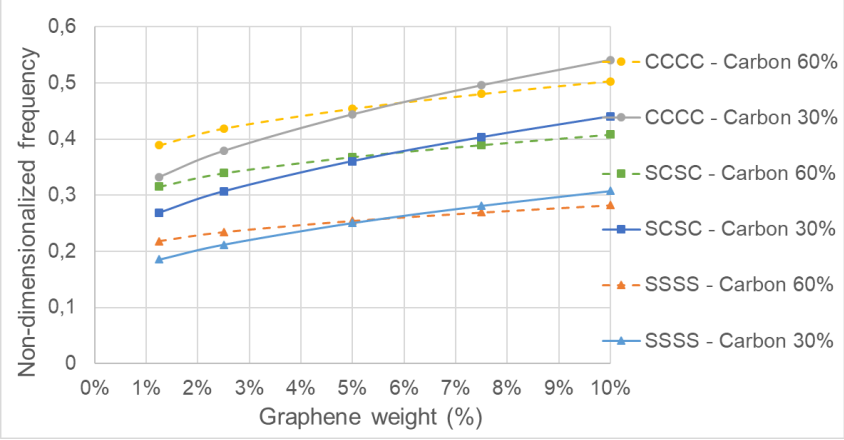

(b)

Fig. 2. Non-dimensional frequencies Ω of 8-layered laminates with uniform graphene and fibre distributions in layers and anti-symmetric stacking sequence $[0/90/0/90]_{\text{anti-s}}$ with $D/a=0.1$, $a/b=1$ for a) glass fibres, b) carbon fibres

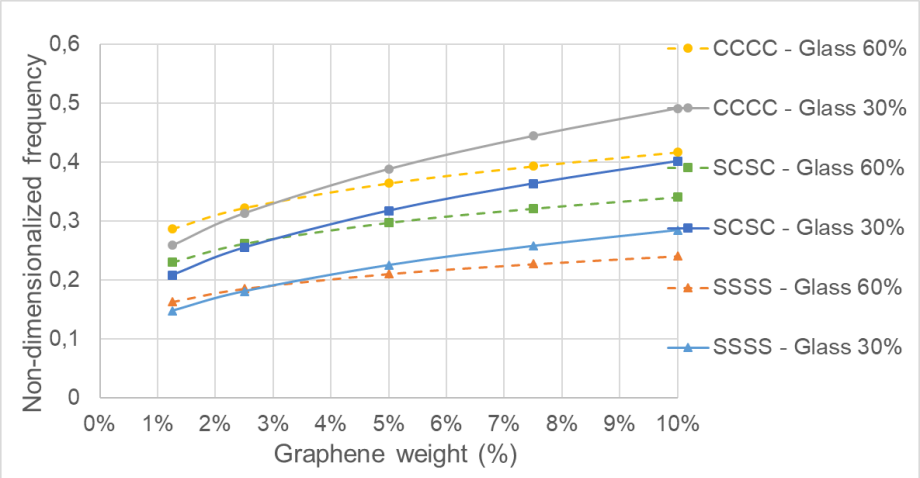

(a)

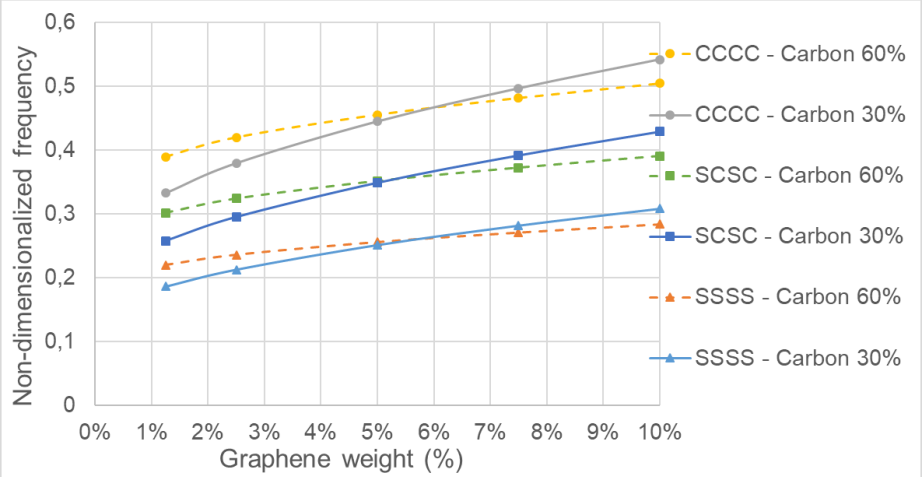

(b)

Fig. 3. Non-dimensional frequencies Ω of 8-layered laminates with uniform graphene and fibre distributions in layers and symmetrical stacking sequence $[90/0/90/0]_s$ with $D/a = 0.1$, $a/b = 1$ for a) glass fibres, b) carbon fibres

It can be observed from Figs. 2 and 3 that as the graphene weight increases beyond a certain limit, a lower percentage of fibres (30%) results in a higher frequency as compared to the higher percentage of fibres (60%) for both glass and carbon fibres. This cross-over point for glass fibres is approximately 3% of graphene weight and for carbon fibres approximately 6% of graphene weight. A physical explanation for this behaviour can be presented, by noting that the contribution of the Young's modulus of the graphene reinforced matrix E_{GM} (Eq. (14)) to E_{11} (Eq. (21)) decreases, as the fibre content V_F increases, due to the second term of Eq. (21) decreasing as V_F increases. Since the graphene reinforced matrix has a high elastic modulus E_{GM}, decrease in the contribution of E_{GM} to E_{11} affects the natural frequency negatively once V_F becomes too high. The

reason for the cross-over point being higher in the case of carbon fibres is due to the high value of Young's modulus of carbon fibres which compensate the decrease in the contribution of E_{GM} as fibre content increases.

This observation indicates that the optimal distribution of graphene and the fibres along the thickness of the laminate needs to be taken into account for an efficient design since a simplified consideration, e.g., of uniform distribution of the graphene reinforcement across the thickness may lead to diminishing returns. Also the results indicate that a higher fibre content does not lead to higher frequencies at higher graphene contents since increasing the fibre content has the effect of reducing the frequency if the graphene content exceeds a certain threshold. It is observed that this threshold value is higher for carbon fibre reinforced laminates as compared to glass fibre reinforced laminates. This effect is due to the higher stiffness of the carbon fibres. It is observed that the two different stacking sequences shown in Figs. 2 and 3, namely, cross-ply anti-symmetric and symmetric, result in similar behaviours.

7. Optimal design results

Optimization results obtained by the maximization of the fundamental frequency are given in this section. Results are presented for three different boundary conditions, namely, simply supported (SSSS), clamped (CCCC) and simply supported and clamped in opposite edges (SCSC). The simulations are conducted for eight-layered laminates and the design variables are the graphene weight and the fibre volume contents of layers, the layer thicknesses, the fibre angles as well as combinations of these variables. The layer thickness ratio is defined as the thickness of the layer over the total thickness of the laminate, i.e., h/D. The ratio of the total thickness of the laminate over the length of one edge is given by D/a and the aspect ratio by a/b.

7.1 Graphene content as the design variable

Next, the design problem for the optimal distribution of GPLs across the thickness is studied with the graphene weight percentages of layers being the only design variables of the problem. This leads to an optimal laminate with the graphene distributed non-uniformly and optimally across the thickness. The design constraint is the maximum GPL weight fraction for the overall laminate, denoted as $W_{GPL\max}$ which is set to 1.25%, i.e.,

$W_{GPL\max} \le 0.0125$. In Table 5, results for optimal graphene content of each layer, maximum frequencies and design efficiency factors are given. The reference frequency Ω_0 corresponds to a laminate with uniform graphene weight equal to 1.25% in all layers.

Table 5: Maximum fundamental frequencies Ω of 8-layered laminates with W_{GPLi} (graphene weight content of i^{th} layer) as the design variables subject to $W_{GPLi} \ge 0$ and $W_{GPL\max} = 1.25\%$ with $D/a = 0.1$, $a/b = 1$ and SSSS boundary conditions

Stacking sequence	**BCs**	**Fibre contents**	**Optimal W_{GPL} per layer**	Ω	$\eta = \frac{\Omega_{\max}}{\Omega_0}$
$[0/90/0/90]_{anti\text{-}s}$	**SSSS**	**Glass 30%**	$[0.048 / 0.0022 / 0 / 0]_s$	0.1766	1.196
		Glass 60%	$[0.036 / 0.014 / 0.0002 / 0]_s$	0.1774	1.091
		Carbon 30%	$[0.047 / 0.003 / 0 / 0]_s$	0.2054	1.108
		Carbon 60%	$[0.033 / 0.013 / 0.004 / 0]_s$	0.2254	1.033
$[90/0/90/0]_s$	**SSSS**	**Glass 30%**	$[0.049 / 0.0017 / 0 / 0]_s$	0.1767	1.196
		Glass 60%	$[0.036 / 0.014 / 0.0001 / 0]_s$	0.1774	1.090
		Carbon 30%	$[0.047 / 0.003 / 0 / 0]_s$	0.2068	1.108
		Carbon 60%	$[0.034 / 0.012 / 0.004 / 0]_s$	0.2275	1.034

Table 5 shows that the outer layers of the laminate have a higher percentage of graphene as compared to the inner layers for optimum design. Since the first eigenmode corresponds to a bending deflection, the (top and bottom) outer layers of the plate influence the response to a higher extend as compared to the middle layers due to the increased contribution of the outer layers to laminate stiffness as compared to the inner layers. Therefore, the optimization algorithm assigns a higher content of reinforcement in the outer layers and less or even zero content of reinforcement in the middle layers, in order to maximize the natural frequency. The same trend is also observed in the majority of the results presented in this article.

For most of the cases shown in Table 5, only the two outer layers (out of the eight layers) get an increased amount of graphene while the middle layers are kept to a small or zero amount of graphene.

The highest increase in the fundamental frequency with respect to the reference frequency is 19.6% corresponding to the laminate with 30% glass fibres for the symmetric and anti-symmetric cases as indicated by the design efficiency index shown in the last column of Table 5. In the case of 30% fibre content (glass or carbon), increase in the frequency is approximately twice or more compared to the case of 60% fibre content. This indicates that in the present case of uniformly distributed fibres across the thickness, a more efficient design is achieved with lower fibre volume contents. As mentioned in section 6, this is attributed to the fact that the increase in the fibre content V_F leads to a decrease in the contribution of E_{GM} to E_{11} as can be observed from Eq. (21).

Moreover, the increase in the frequency (design efficiency) is higher for glass fibres than for carbon fibres. Also Table 5 indicates that symmetric and anti-symmetric stacking sequences have not produced significantly different results.

To investigate the effect of increasing the allowable graphene weight for the overall laminate (W_{GPLmax}) on the design efficiency, three different values of W_{GPLmax}, equal to 1.25%, 2.5% and 5%, have been studied as shown in Fig. 4. The fibre volume contents across the thickness were kept uniform as before.

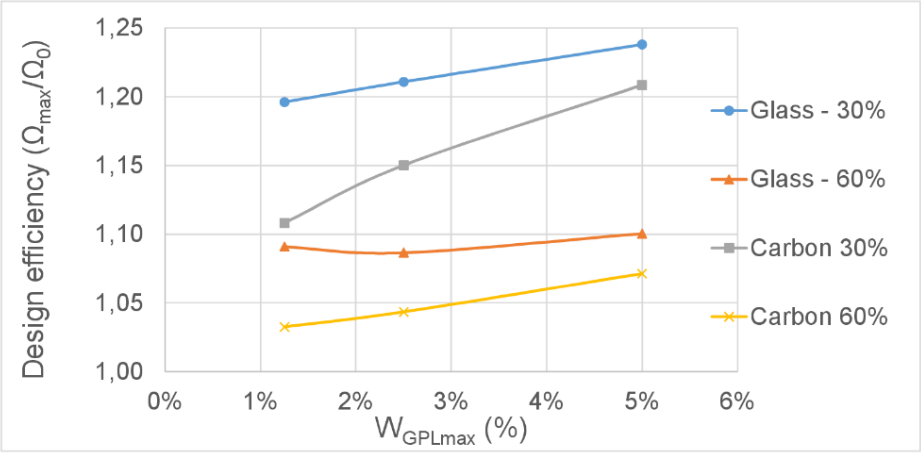

Fig. 4. Design efficiency vs $W_{GPL\,\max}$ for different fibres and fibre contents with SSSS boundary conditions and $[0/90/0/90]_{anti\text{-}s}$ laminates

Fig. 4 indicates that increasing the total graphene weight is more efficient when a lower fibre content is used. For glass fibres with 60% fibre content, increasing the maximum graphene weight has almost no effect on the design efficiency. Results show that when a

uniform fibre distribution is adopted, non-uniform distribution of graphene across the thickness leads to higher frequencies. The corresponding design efficiency factor becomes higher when lower fibre volume contents are used. An increase in the fibre content or use of carbon instead of glass result in increased frequency. However, this leads to lower design efficiency.

7.2 Graphene and fibre contents as design variables

Next, optimal designs with two sets of design variables are considered, namely, the optimal distributions of GPLs and fibres across the thickness. The results are shown in Table 6. The maximum graphene content for the overall laminate $W_{GPL\max}$ is set to 1.25% and the maximum fibre volume content $V_{F\max}$ to 30%. The reference frequency Ω_0 to compute the design efficiency corresponds to a uniform graphene content of 1.25% and a uniform fibre content of 30% for all layers.

Table 6: Maximum fundamental frequencies Ω of 8-layered laminates with two design variables: graphene and fibre contents (W_{GPLi}, V_{Fi}) of layers subject to $W_{GPLi} \geq 0$, $0.1 \leq V_{Fi} \leq 0.6$, $W_{GPL\max} = 1.25\%$, $V_{F\max} = 30\%$ with $D/a = 0.1$, $a/b = 1$ and stacking sequence $[0/90/0/90]_{\text{anti-s}}$

BCs	Fibres	Optimal W_{GPL}	Optimal V_F	Ω	$\eta = \frac{\Omega_{\max}}{\Omega_0}$
SSSS	**Glass**	$[0.035 / 0.015 / 0 / 0]_s$	$[0.6 / 0.4 / 0.1 / 0.1 /]_s$	0.1864	1.262
	Carbon	$[0.042 / 0.008 / 0 / 0]_s$	$[0.4 / 0.6 / 0.1 / 0.1 /]_s$	0.2209	1.192
CCCC	**Glass**	$[0.032 / 0.018 / 0 / 0]_s$	$[0.6 / 0.4 / 0.1 / 0.1]_s$	0.3113	1.202
	Carbon	$[0.027 / 0.014 / 0.009 / 0]_s$	$[0.48 / 0.52 / 0.1 / 0.1]_s$	0.3709	1.117
SCSC	**Glass**	$[0.033 / 0.018 / 0 / 0]_s$	$[0.6 / 0.4 / 0.1 / 0.1]_s$	0.2566	1.216
	Carbon	$[0.039 / 0.011 / 0 / 0]_s$	$[0.4 / 0.6 / 0.1 / 0.1]_s$	0.3045	1.132

In most cases, as shown in Table 6, a higher graphene content is allocated to the two outer layers while zero graphene weight is allocated to the middle layers. For carbon fibres

and CCCC boundary conditions, the top and bottom three layers have higher graphene content while only two middle layers have zero graphene content. Concerning the optimal fibre content, all boundary conditions result in higher fibre content in the two outer layers with the middle layers having the minimum fibre content as dictated by the constraint on minimum fibre content. Similar to the discussion presented in section 7.1, the optimization algorithm assigns a higher reinforcement content to the outer layers due to these layers affecting the structural response of the laminate more than the middle layers.

In the case of carbon fibres, it seems that values of fibre volume contents for the outer layers depend on the type of the boundary conditions. Design efficiency is observed to be the highest for glass fibres and SSSS boundary conditions (26.2%), followed by SCSC (21.6%) and CCCC (20.2%). For carbon fibres, highest efficiencies are obtained for SSSS (19.2%), followed by SCSC (13.2%) and CCCC (11.7%). Thus, as the boundary conditions become more stiff (from SSSS to CCCC), less space is left for improvement of the natural frequency, which results in the decrease of the design efficiency. Comparing Tables 5 and 6, it is observed that design efficiency index in Table 6 indicates an increase of 26.2% for glass fibres and 19.2% for carbon fibres for SSSS boundary conditions. The corresponding increases for the case of uniform fibre distributions shown in Table 5 are 19.6% and 10.8%, respectively, indicating that optimal non-uniform fibre distribution results in significantly increased frequencies for both glass and carbon fibres. It is noted that in both cases the same amount of total fibre content for the laminate is specified.

Therefore, this increase in the design efficiency in the case of non-uniform fibre (and graphene) distributions is due to the fact that optimization distributes the fibre reinforcement optimally by assigning a higher fibre content in the outer layers and a lower fibre content in the middle layers as compared to the case of a uniform fibre distribution presented in Table 5.

To investigate the sensitivity of the frequency to design parameters, contour plots with respect to graphene and fibre contents are drawn as shown in Fig. 5 for SSSS boundary conditions. In Fig. 5, the two horizontal axes indicate the variation of the graphene weight and fibre volume contents of the outer (surface) layers of the 8-layered laminate. The values of the graphene and fibre contents of the intermediate layers (layers 2 to 7) are taken from the optimization results shown in Table 6.

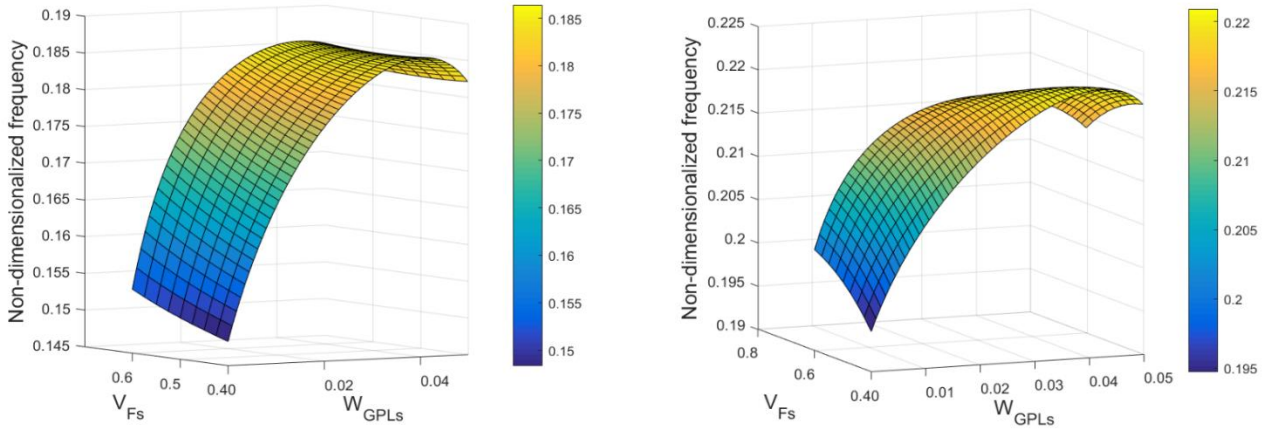

(a) (b)

Fig 5. Contour plots of frequency for SSSS boundary conditions with varying graphene weight and fibre volume contents of the surface layers for a) glass and b) carbon fibres

Both Figs. 5a and 5b indicate that there is an optimal graphene weight for the outer layer which maximizes the frequency. Exceeding this optimal value of the graphene weight leads to a decrease in the frequency. In the case of glass fibres (Fig. 5a), the maximum frequency is not sensitive to the change in the fibre volume content. However, for carbon fibres (Fig. 5b), when the graphene content is high, the lower fibre content results in higher frequency and increasing the fibre content results in lower frequency.

For glass fibres and CCCC or SCSC boundary conditions, similar patterns for the contour plots were observed. For carbon fibres and CCCC boundary conditions, the contour plot shown in Fig. 6a indicates that frequency is quite sensitive to change in the graphene weight around the maximum frequency as compared to SSSS boundary conditions (Fig. 5b). This becomes more pronounced for higher fibre volume contents and for the (more stiff) CCCC boundary conditions, followed by the SCSC boundary conditions (Fig. 6b).

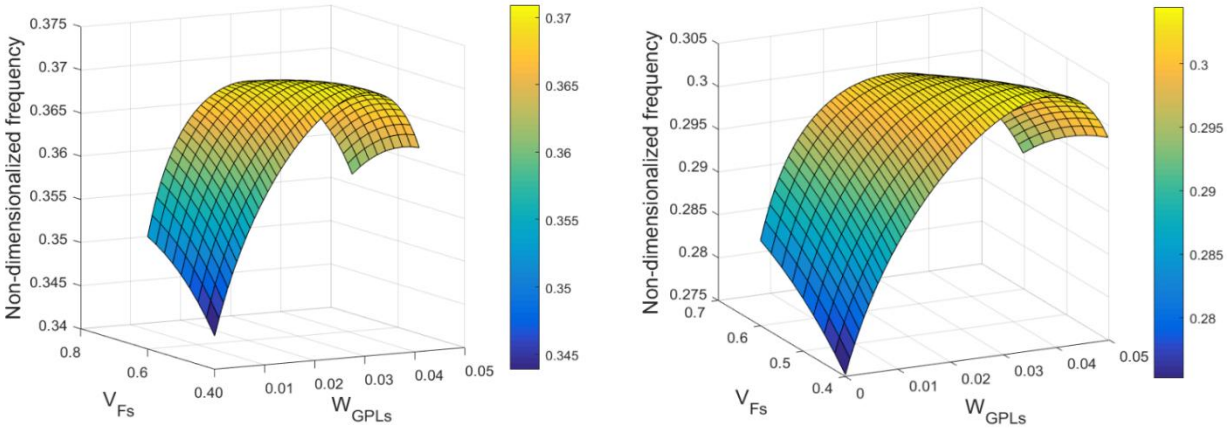

(a) (b)

Fig. 6. Contour plots of the frequency for carbon fibre reinforced laminates with varying graphene weight and fibre volume contents of the outer layers for a) CCCC and b) SCSC boundary conditions

To further investigate the contribution of graphene on maximizing the frequency, additional simulations with zero graphene weight have been performed. Two design efficiency factors are calculated for this case: a) $\eta = \frac{\Omega_{max}}{\Omega_0}$ where Ω_{max} is the optimal frequency and Ω_0 the reference frequency obtained for non-zero, uniform graphene weight equal to 1.25% for all the layers of the laminate and b) $\eta_2 = \frac{\Omega_{max}}{\Omega_{02}}$ where the reference frequency Ω_{02} is obtained for zero graphene weight. The design efficiency factor η_2 shown in Table 7 indicates a significant increase of the fundamental frequency when the fibres are distributed optimally among the layers as compared to the frequency of a laminate with uniformly distributed fibres. The increase is observed to be greater in the case of glass fibre reinforced laminates as compared to the carbon fibre reinforced ones. When the efficiency factor η is examined in Table 7, it is observed that a significant reduction in the maximum frequency occurs in the absence of graphene reinforcement noting that the reference frequency Ω_0 refers to a laminate with uniformly distributed graphene of 1.25% volume content. The highest reduction in the frequency is observed in the case of glass fibres and CCCC and SCSC boundary conditions and it is equal to (1-0.727)/100 = 27.3%. A more holistic insight on the positive contribution of the non-uniform distribution of graphene across the laminate thickness can be obtained by comparing the design efficiency factors in Table 6 (non-zero, non-uniform graphene distribution along thickness) and the factor η of Table 7 (zero graphene). Both factors are calculated using the same reference frequency Ω_0 which corresponds to uniform graphene distribution with a weight

content of 1.25% for all layers. For glass fibres and CCCC boundary conditions, Table 6 indicates an increase of 20.2% of the maximum frequency with respect to the reference frequency. For the same case (glass fibres and CCCC), the reduction in the fundamental frequency with respect to the reference frequency Ω_0 obtained from Table 7 (1-0.727)/100 = 27.3%), a total increase equal to 20.2% + 27.3% = 47.5% of the optimal fundamental frequency with non-uniform graphene distribution arises, in comparison to zero graphene usage. Significant improvements in the vibration response also arise when the proposed non-uniform graphene distribution shown in Table 6 is used for all the cases presented in Tables 6 and 7.

Table 7: Maximum fundamental frequencies Ω of 8-layered laminates with zero graphene content and design variables as the fibre contents $V_{F\,i}$ of layers subject to $0.1 \le V_{Fi} \le 0.6$, $V_{F\max} = 30\%$ with $D/a = 0.1,\ \ a/b = 1$ and stacking sequence $[0/90/0/90]_{\text{anti-s}}$

BCs		Optimal V_F	Ω	$\eta = \frac{\Omega_{\max}}{\Omega_0}$	$\eta_2 = \frac{\Omega_{\max}}{\Omega_{02}}$
SSSS	Glass	$[0.6 / 0.4 / 0.1 / 0.1]_s$	0.1079	0.731	1.202
	Carbon	$[0.57 / 0.43 / 0.1 / 0.1]_s$	0.1611	0.869	1.167
CCCC	Glass	$[0.6 / 0.4 / 0.1 / 0.1]_s$	0.1883	0.727	1.165
	Carbon	$[0.6 / 0.4 / 0.1 / 0.1]_s$	0.2508	0.755	1.113
SCSC	Glass	$[0.6 / 0.4 / 0.1 / 0.1]_s$	0.1533	0.727	1.173
	Carbon	$[0.6 / 0.4 / 0.1 / 0.1]_s$	0.2103	0.782	1.127

To better represent the aforementioned improvement of the vibration behaviour of the composite laminate when a non-uniform graphene distribution is adopted, Fig. 7 represents the $(\Omega_{max}-\Omega_0)/\Omega_0$ (%) vs boundary conditions diagrams, obtained from Tables 6 and 7. The top line in each diagram represents the increase of the maximum frequency for the non-uniform graphene distribution shown in Table 6 with respect to the reference frequency (non-zero, uniform graphene) for glass and carbon fibres. The bottom line shows the corresponding percentage, representing the decrease of the maximum frequency obtained for zero graphene with respect to the reference frequency (non-zero,

uniform graphene). The figure indicates that a significant increase of the fundamental frequency corresponding to the non-uniform graphene distribution is observed for all cases as compared to zero graphene content. For glass fibres, this increase may reach 51% (SSSS) and is not less than 46% (CCCC). For carbon fibres the maximum increase is 36% (CCCC) and the minimum 30% (SSSS).

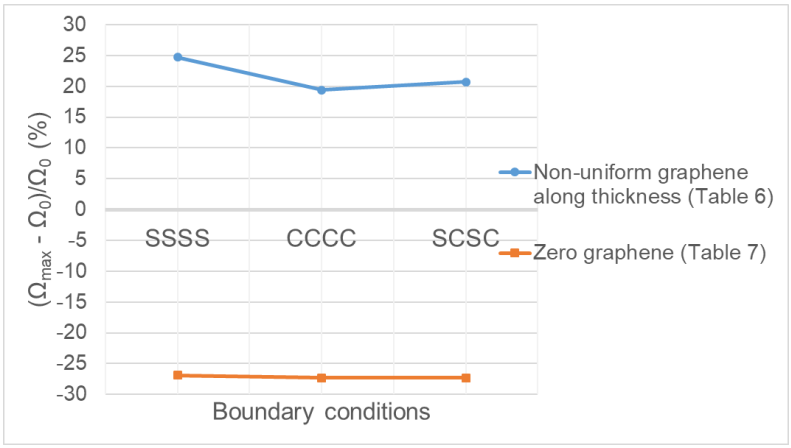

(a)

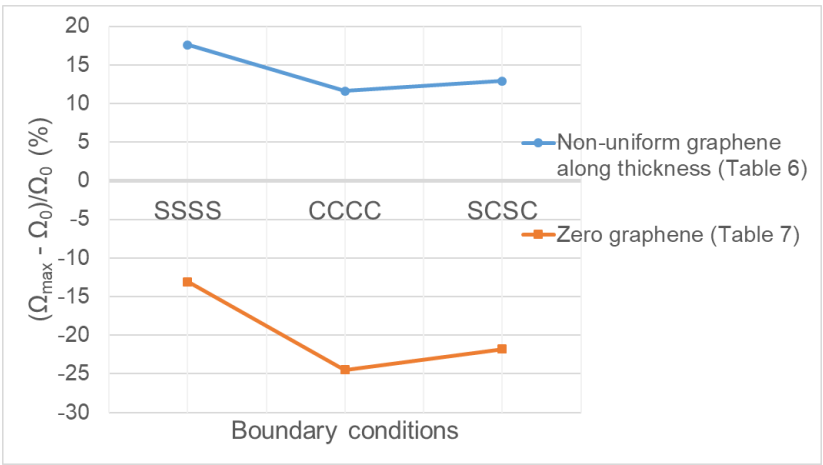

(b)

Fig. 7. Comparison between the maximum and the reference frequencies for three boundary conditions and a) glass, b) carbon fibres

7.3 Graphene and fibre contents and layer thicknesses as design variables

Next, in addition to the two design variables of graphene and fibre contents studied so far, another design variable, namely, the layer thicknesses are included as design variables. This leads to optimal design for maximum frequency with three design variables. The results of the optimization with these design variables are shown in Tables 8, 9 and 10 corresponding to the three boundary conditions of SSSS, CCCC and SCSC, respectively.

Table 8: Maximum fundamental frequencies Ω of 8-layered laminates with three design variables subject to $W_{GPLi} \geq 0$, $0.1 \leq V_{Fi} \leq 0.6$, $0.01 \leq h_i / D \leq 0.15$, $W_{GPL\max} = 1.25\%$, $V_{F\max} = 30\%$ with $D/a = 0.1$, $a/b = 1$ and SSSS boundary conditions

Stacking sequence	Fibres	Optimal W_{GPL}	Optimal V_F	h_i/D	Ω	$\eta = \frac{\Omega_{\max}}{\Omega_0}$
$[0/90/0/90]_{anti\text{-}s}$	**Glass**	$[0.042/0.021/0/0]_s$	$[0.6/0.6/0.1/0.1]_s$	$[0.095/0.105/0.15/0.15]_s$	0.1892	1.281
	Carbon	$[0.041/0.02/0.003/0]_s$	$[0.6/0.6/0.1/0.1]_s$	$[0.08/0.12/0.15/0.15]_s$	0.2244	1.211
$[90/0/90/0]_s$	**Glass**	$[0.043/0.021/0/0]_s$	$[0.6/0.6/0.1/0.1]_s$	$[0.094/0.106/0.15/0.15]_s$	0.1892	1.280
	Carbon	$[0.043/0.021/0.003/0]_s$	$[0.6/0.6/0.1/0.1]_s$	$[0.07/0.13/0.15/0.15]_s$	0.2244	1.203

Table 9: Maximum fundamental frequencies Ω of 8-layered laminates with three design variables subject to $W_{GPLi} \geq 0$, $0.1 \leq V_{Fi} \leq 0.6$, $0.01 \leq h_i / D \leq 0.15$, $W_{GPL\max} = 1.25\%$. $V_{F\max} = 30\%$ with $D/a = 0.1$, $a/b = 1$ and CCCC boundary conditions

Stacking sequence	Fibres	Optimal W_{GPL}	Optimal V_F	h_i/D	Ω	$\eta = \frac{\Omega_{\max}}{\Omega_0}$
$[0/90/0/90]_{anti\text{-}s}$	**Glass**	$[0.041/0.023/0/0]_s$	$[0.6/0.6/0.1/0.1]_s$	$[0.09/0.11/0.15/0.15]_s$	0,3146	1.214
	Carbo	$[0.019/0.014/0.021/0]_s$	$[0.6/0.6/0.1/0.1]_s$	$[0.08/0.12/0.15/0.15]_s$	0.3802	1.145
$[90/0/90/0]_s$	**Glass**	$[0.041/0.023/0/0]_s$	$[0.6/0.6/0.1/0.1]_s$	$[0.09/0.11/0.15/0.15]_s$	0,3146	1.214
	Carbo	$[0.103/0.008/0/0]_s$	$[0.1/0.6/0.27/0.1]_s$	$[0.05/0.15/0.15/0.15]_s$	0.3794	1.141

Table 10: Maximum fundamental frequencies Ω of 8-layered laminates with three design variables subject to $W_{GPLi} \geq 0$, $0.1 \leq V_{Fi} \leq 0.6$, $0.01 \leq h_i / D \leq 0.15$, $W_{GPL\max} = 1.25\%$, $V_{F\max} = 30\%$ with $D/a = 0.1$, $a/b = 1$ and SCSC boundary conditions

Stacking sequence	Fibres	Optimal W_{GPL}	Optimal V_F	Optimal h_i/D	Ω	$\eta = \frac{\Omega_{\max}}{\Omega_0}$
$[0/90/0/90]_{anti\text{-}s}$	**Glass**	$[0.041/0.023/0/0]_s$	$[0.6/0.6/0.1/0.1]_s$	$[0.09/0.11/0.15/0.15]_s$	0.2595	1.230
	Carbon	$[0.109/0.006/0/0]_s$	$[0.1/0.6/0.27/0.1]_s$	$[0.05/0.15/0.15/0.15]_s$	0.3082	1.146
$[90/0/90/0]_s$	**Glass**	$[0.057/0.014/0/0]_s$	$[0.45/0.6/0.1/0.1]_s$	$[0.07/0.15/0.13/0.15]_s$	0.2614	1.254
	Carbon	$[0.093/0.011/0/0]_s$	$[0.1/0.6/0.27/0.1]_s$	$[0.05/0.15/0.15/0.15]_s$	0.3282	1.272

Comparison between the results presented in Tables 8-10 (including non-uniform layer thicknesses) and Table 6 (with uniform layer thicknesses) indicates that the efficiency factor increases with the addition of layer thicknesses to design variables as expected. The minimum increase is 1.2% (CCCC-glass fibres) and the maximum increase is 2.8% (CCCC-carbon fibres). In the majority of the cases, the layers close to laminate surface receive a higher graphene content with an increase in the thicknesses of the middle layers. Thus, the optimal designs correspond to a reduced thickness in the surface layers which have increased graphene content compared to the cases of uniform layer thicknesses as observed in Table 6.

Moreover, for SCSC boundary conditions and carbon fibres, the symmetric stacking sequence results in significantly higher efficiency factor as compared to the anti-symmetric case. For the other boundary conditions, both stacking sequences result in similar efficiency factors.

7.4 Graphene and fibre contents, layer thicknesses and fibre orientations as design variables

In view of the importance of fibre orientations in the design of composite laminates, fibre angles are now introduced as the fourth set of design variables in addition to graphene and fibre contents and layer thicknesses. This leads to an optimal design problem with four design variables.

Table 11: Maximum fundamental frequencies Ω of 8-layered laminates with four design variables subject to $W_{GPLi} \geq 0$, $0.1 \leq V_{Fi} \leq 0.6$, $0.01 \leq h_i / D \leq 0.15$, $-90° \leq \theta_i \leq 90°$, $W_{GPL\max} = 1.25\%$, $V_{F\max} = 30\%$ with $D/a = 0.1$, $a/b = 1$

Boundary conditions	**Fibres**	**Optimal W_{GPL}**	**Optimal V_F**	***h_i/D***	θ_i	**Ω**	$\eta = \frac{\Omega_{\max}}{\Omega_0}$
SSSS	**Glass**	[0.110/0.005/ 0/0]$_s$	[0.10/0.60/ 0.27/0.10]$_s$	[0.05/0.15 /0.15/0.15]$_s$	[45/-45/45/45]$_s$	0.2006	1.359
	Carbon	[0.119/0.003/ 0/0]$_s$	[0.10/0.60/ 0.27/0.10]$_s$	[0.05/0.15/ 0.15/0.15]$_s$	[45/-45/45/45]$_s$	0.2586	1.395
CCCC	**Glass**	[0.041/0.023/ 0/0]$_s$	[0.6/0.6/ 0.1/0.1]$_s$	[0.09/0.11/ 0.15/0.15]$_s$	[0/90/0/90]$_s$	0.3146	1.214
	Carbon	[0.019/0.014/ 0.021/0]$_s$	[0.6/0.6/ 0.1/0.1]$_s$	[0.07/0.13/ 0.15/0.15]$_s$	[0/90/0/90]$_s$	0.3802	1.145
SCSC	**Glass**	[0.057/0.015/ 0/0]$_s$	[0.46/0.6/ 0.1/0.1]$_s$	[0.07/0.15/ 0.15/0.13]$_s$	[0/0/0/0]$_s$	0.2625	1.244
	Carbon	[0.087/0.012/ 0.001/0]$_s$	[0.10/0.60/ 0.27/0.10]$_s$	[0.05/0.15/ 0.15/0.15]$_s$	[0/0/0/0]$_s$	0.3372	1.254

Results of this optimization problem are shown in Table 11. It is observed that the optimal designs for different boundary conditions result in different stacking sequences as expected. Similar to the previous cases, higher graphene weights are allocated to outer layers. Comparison between the results presented in Tables 8-10 (cross-ply laminates) indicates a further increase of the fundamental frequency for SSSS and SCSC boundary conditions. This increase is quite significant for SSSS boundary conditions (+ 7.8% for glass and +18.4% for carbon fibres) and for SCSC-carbon fibres (+10.8%). It is noted that the design efficiency factors shown in Table 11 are calculated for a reference frequency obtained by using the anti-symmetric, cross-ply stacking sequence, and therefore efficiency comparisons between Table 11 and Tables 8-10 are based on this stacking sequence. For CCCC boundary conditions no increase of the design efficiency is observed, indicating that the cross-ply stacking sequence used in Table 9 results in the optimal vibration response.

A final investigation is conducted by assessing the effect of the variation of the fibre angles of the two outer layers on the fundamental frequency and the corresponding sensitivities. The reason the top two outer layers are chosen for this purpose is because the outer layers contribute most to the stiffness of the laminate. This work is done by means of contour plots of the frequencies with respect to fibre orientations. In the contour plots shown in Figs 8-10, the problem parameters have been assigned their optimal values presented in Table 11 in all layers except the top two outer layers. Thus, the only parameters which vary in these plots are the fibre angles of the outer layers, that is, θ_1 and θ_8 of the top and bottom layers, and θ_2 and θ_7 of the second outer layers.

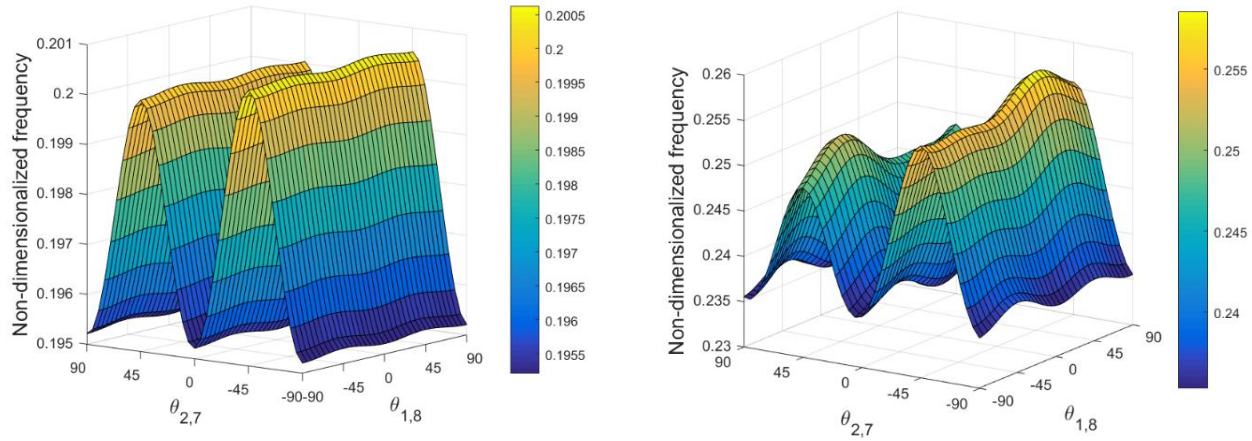

(a) (b)

Fig 8. Contour plots of the frequency with respect to the fibres angles of the two outer layers for SSSS boundary conditions, a) glass fibres, b) carbon fibres

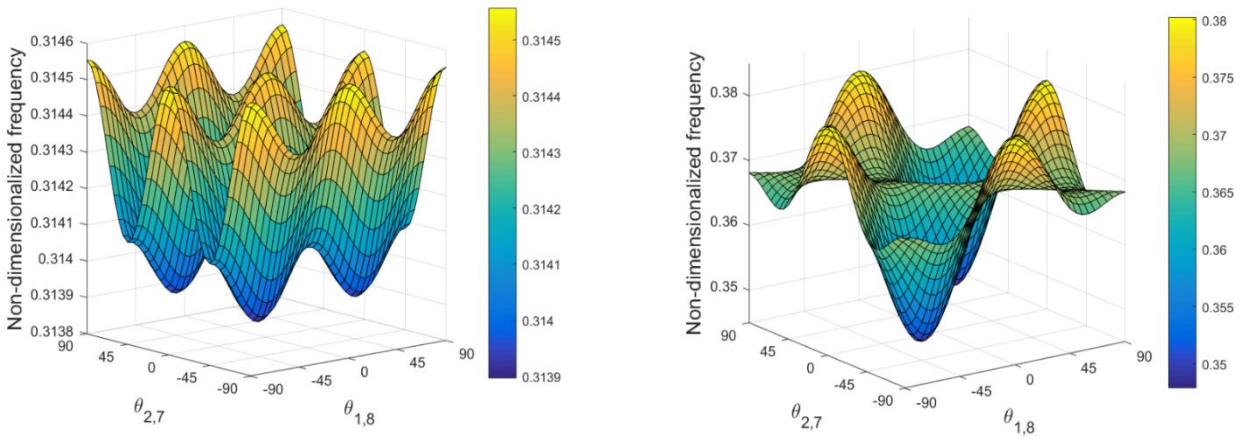

(a) (b)

Fig 9. Contour plots of the frequency with respect to the fibres angles of the two outer layers for CCCC boundary conditions, a) glass fibres, b) carbon fibres

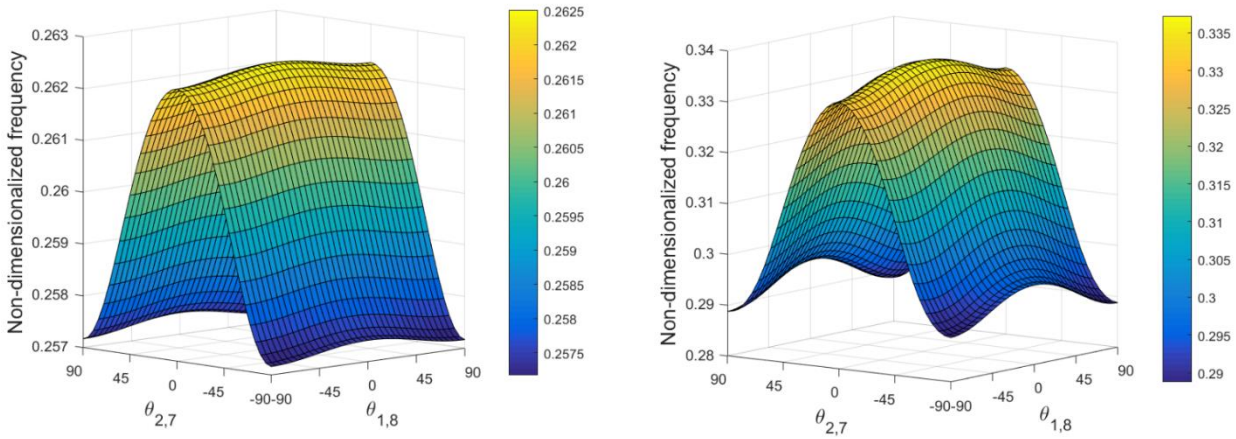

(a) (b)

Fig 10. Contour plot of the frequency with respect to the fibres angles of the two outer layers for SCSC boundary conditions, a) glass fibres, b) carbon fibres

Comparisons between the optimal solutions presented in Table 11 and Figs 8-10 confirms the optimization solution and the corresponding angles $\theta_{1,8}$ and $\theta_{2,7}$ in every case. It is also observed that different boundary conditions result in different shapes of the contour plots as expected. Thus CCCC boundary conditions lead to multiple optimal points. For SSSS and SCSC boundary conditions, a single optimal point is observed and this point is more prominent in the case of carbon fibre reinforced laminates. This leads to the observation that when glass fibres are used for reinforcement, the difference between the minimum and the maximum values of the frequency is relatively small as compared to the case of carbon fibres.

8. Conclusions

Optimal design and analysis of a hybrid graphene/fibre reinforced composite laminate for maximum fundamental frequency was the subject of the present study. The composite material is defined as a three-phase nanocomposite consisting of graphene nanoplatelets, fibres and polymer matrix. The main objective was the study of the vibration response and optimization of this multiscale laminate combining a nano-scale reinforcement (graphene) within the traditional fibre reinforced matrix and the effect of the graphene content on the maximum frequency. To achieve a cost-effective design, the optimal distributions of the constituent materials along the thickness of the structure as well as optimal layer thicknesses are investigated to maximize the fundamental frequency.

For the implementation of the optimization scheme, a Sequential Quadratic Programming algorithm (SQP) was adopted. The natural vibration problem is solved within the framework of the finite element method using the First Order Shear Deformation plate theory (FSDT). Three different boundary conditions, namely, SSSS, CCCC and SCSC are investigated to assess their effect on the optimal designs. Effective properties of three-phase composite are obtained from micromechanics equations applicable to graphene and fibre reinforced polymers. The numerical results are given for symmetric and anti-symmetric 8-layered laminates.

Among the main findings of the study is the optimal distributions of graphene and fibre reinforcements along the thickness of the laminate. It is observed that a non-uniform distribution of graphene platelets, with higher graphene contents in the surface layers and lower or zero graphene contents in the middle layers, results in the optimal distribution of the graphene. When the fibre volume contents are also included as design variables, a similar pattern of optimal fibre distribution is observed, that is, higher fibre contents in the outer layers and the less fibre content in the middle layers.

A design efficiency factor is introduced which is defined as the ratio of the fundamental frequency of the optimally designed laminate over a reference frequency based on uniform distributions of the reinforcements and uniform layer thicknesses. This provides a quantitative measurement of the positive effect of the non-uniformly distributed reinforcements leading to optimal designs. When the layer thicknesses and the fibre angles are also included as design variables of the optimization problem, the design efficiency factors indicate a further increase in the fundamental frequency as expected.

Some specific conclusions are presented below:

a) Increasing graphene weight is more effective in improving the fundamental frequencies for lower fibre volume contents (Figs 2 and 3).

b) When the graphene contents of layers are the only design variables of the optimization problem and a uniform fibre distribution along the thickness is adopted, a higher graphene content results in the outer layers as expected. The highest increase of the fundamental frequency with respect to the reference frequency is 19.6%. This corresponds to a symmetric cross-ply laminate with glass fibres of 30% volume content. The corresponding increase when 30% of carbon fibres is used is 10.8%. This is due to the fact that glass fibres have lower stiffness and graphene becomes more effective in improving the maximum frequency while carbon fibres have higher stiffness and addition of graphene is, relatively speaking, not as efficient as it was in the case of glass fibres.

c) For the case of optimal distribution of graphene (same as case b), the increase in the fundamental frequency when fibre volume content is 60% (instead of 30% as in case b), is half in the case of glass fibre reinforcement and one third for carbon fibre reinforcement. This indicates that the graphene reinforcement is more efficient at lower fibre contents.

d) It was observed that a higher design efficiency factor was obtained when glass instead of carbon fibres are used. This is attributed to the lower stiffness of glass fibres which results in higher contribution of graphene platelets to the fundamental frequency.

e) When both graphene and fibre reinforcements are specified as design variables, a non-uniform distribution along the thickness arises for both reinforcements. The optimal non-uniform fibre distributions result in significantly increased frequencies in comparison to uniform fibre distributions.

f) The highest increase of the fundamental frequency with respect to the reference frequency is 26.2% in the case of SSSS boundary conditions. CCCC boundary conditions result in the lowest increase in the design efficiency. This can be attributed to the fact that for CCCC boundary conditions, the fundamental frequencies are already relatively high compared to the case of SSSS boundary conditions.

g) When zero and non-zero graphene reinforcements are compared, results indicate that a large increase in the fundamental frequency is observed relative to case with zero graphene content compared to the case of non-uniformly distributed graphene. This increase reaches 51% in the case of additional reinforcements with glass fibre and 36% with carbon fibres.

h) When the layer thicknesses are specified as further design variables (in addition to graphene and fibre volume contents), a relatively small increase in the design efficiency factor is observed which is 1.2% for CCCC-glass fibres and 2.8% for CCCC-carbon fibres.

i) For the case of three design variables involving graphene and fibre contents of layers and the layer thicknesses, the fundamental frequency is 28.1 % higher compared to the reference frequency in the case of glass fibre reinforced laminates with SSSS boundary conditions compared to 26.2% for the case of uniform layer thickness (two sets of design variables). The corresponding increase is 19.6% in the case of uniform layer thicknesses and uniform fibre contents with the graphene contents of layers being the only design variables.

j) When the fibre angles are also included as the design variables in addition to the previous set of three design variables (graphene and fibre contents and thicknesses of layers), a significant increase in the design efficiency factor is observed. These increases

are 7.8% for GFRP and 18.4% for CFRP laminates with SSSS boundary conditions. and 10.8% for CFRP laminates with SCSC boundary conditions.

k) For this case (four sets of design variables) and SSSS boundary conditions, the increase of the fundamental frequency with respect to the reference frequency reaches 35.9% for GFRP and 39.5% for CFRP laminates.

Future research on three-phase nanocomposites is to include the investigation of functionally graded nanomaterials where the graphene weight varies along the thickness of the laminate which may be a pre-defined distribution or an optimally determined continuous distribution. In addition, a non-constant graphene distribution in each layer may also result in an improved design and a cost-effective use of the expensive graphene reinforcement. Finally, more advanced theories and bounds for the micromechanical formulations presented in literature [67, 68], can be adopted and compared for three-phase composites.

References

1. Ebrahimi F (Ed.). Nanocomposites - New Trends and Developments. Intech, Rijeka, Croatia, 2012.

2. Reddy B. (Ed.). Advances in Diverse Industrial Applications of Nanocomposites. Intech, Rijeka, Croatia, 2011.

3. Gao F. (Ed.). Advances in polymer nanocomposites - Types and applications. Woodhead Publishing Limited, Cambridge, UK, 2012.

4. Mittal V. (Ed.). Polymer-Graphene Nanocomposites. The Royal Society of Chemistry 2012, Cambridge, UK.

5. Zhao S, Zhao Z, Yang Z, Ke L, Kitipornchai S, Yang J. Functionally graded graphene reinforced composite structures: A review. Eng Struct 2020;210:110339.

6. Mohan VB, Lau K, Hui D, Bhattacharyya D. Graphene-based materials and their composites: A review on production, applications and product limitations, Compos Part B: Eng 2018;1421:200-220.

7. Tairidis GK, Foutsitzi G, Stavroulakis GE. Optimal design of smart composites. In Demetriou IC, Pardalos PM, editors. Approximation and Optimization. Algorithms, Complexity and Applications. Springer, Cham, 2019.

8. Narita Y. Layerwise optimization for the maximum fundamental frequency of laminated composite plates. J Sound Vib 2003;263(5):1005–1016.

9. Liu Q. Exact sensitivity analysis of stresses and lightweight design of Timoshenko composite beams. Compos Struct 2016;143: 272-286.

10. Kuo S-Y. Thermal buckling, vibration and flutter of composite laminates containing two non-uniformly distributed fibers. Journal of Aeronautics, Astronautics and Aviation 2016;48(3):173-182.

11. Vo-Duy T, Ho-Huu V, Do-Thi TD, Dang-Trung H, Nguyen-Thoi T. A global numerical approach for lightweight design optimization of laminated composite plates subjected to frequency constraints. Compos Struct 2017;159:646–655.

12. Shi G, Araby S, Gibson CT, Meng Q, Zhu S, Ma J. Graphene platelets and their polymer composites: fabrication, structure, properties and applications. Advanced Functional Materials 2018;28(19):1-44.

13. Cataldi P, Athanassiou A, Bayer I. Graphene nanoplatelets-based advanced materials and recent progress in sustainable applications. Applied Sciences 2018;8(9):1-35.

14. Ray SC. Applications of Graphene and Graphene-Oxide Based Nanomaterials. Elsevier, Oxford, UK, 2015.

15. Lee C, Wei X, Kysar JW, Hone J. Measurement of the elastic properties and intrinsic strength of monolayer graphene. Science 2008;321(5887):385-8.

16. Rafiee MA, Rafiee J, Wang Z, Song H, Yu Z-Z, Koratkar N. Enhanced mechanical properties of nanocomposites at low graphene content. ACS Nano 2009;3(12):3884-90.

17. Tang LC, Wan YJ, Yan D, Pei YB, Zhao L, Li YB, et al. The effect of graphene dispersion on the mechanical properties of graphene/epoxy composites. Carbon 2013;60:16–27.

18. Young RJ, Liu M, Kinloch IA, Li S, Zhao X, Vallés C, Papageorgiou DG. The mechanics of reinforcement of polymers by graphene nanoplatelets. Composites Science and Technology 2018;154:110–116.

19. Thai CH, Ferreira AJM, Tran TD, Phung-Van P. Free vibration, buckling and bending analyses of multilayer functionally graded graphene nanoplatelets reinforced composite plates using the NURBS formulation. Compos Struct 2019;220:749-759.

20. Mohamad N, Yaakub J, Ab Maulod HE, Jeefferie AR, Yuhazri MY, Lau KT, et al. Vibrational damping behaviors of graphene nanoplatelets reinforced NR/EPDM nanocomposites, Journal of Mechanical Engineering and Sciences 2017;11:3274-3287.

21. Duffy KJ, Adali S. Optimal fibre orientation of antisymmetric hybrid laminates for maximum fundamental frequency and frequency separation. J Sound Vib 1991;146 (2):181-190.

22. An H, Chen S, Huang H. Multi-objective optimal design of hybrid composite laminates for minimum cost and maximum fundamental frequency and frequency gaps. Compos Struct 2019;209:268-276.

23. Pashmforoush F. Statistical analysis on free vibration behavior of functionally graded nanocomposite plates reinforced by graphene platelets. Compos Struct 2019;213:14-24.

24. Feng C, Kitipornchai S, Yang J. Nonlinear free vibration of functionally graded polymer composite beams reinforced with graphene nanoplatelets (GPLs). Eng Struct 2017;140:110–119.

25. Rout M, Hota SS, Karmakar A. Thermoelastic free vibration response of graphene reinforced laminated composite shells. Eng Struct 2019;178:179–190.

26. Reddy RMR, Karunasena W, Lokuge W. Free vibration of functionally graded-GPL reinforced composite plates with different boundary conditions. Aerosp Sci Technol 2018;78:147–156.

27. Guo H, Cao S, Yang T, Chen Y. Vibration of laminated composite quadrilateral plates reinforced with graphene nanoplatelets using the element-free IMLS-Ritz method. Int J Mech Sci 2018;142:610–621.

28. Gholami R, Ansari R. Nonlinear harmonically excited vibration of third-order shear deformable functionally graded graphene platelet-reinforced composite rectangular plates. Eng Struct 2018; 156:197–209.

29. Xu Z, Huang Q. Vibro-acoustic analysis of functionally graded graphene-reinforced nanocomposite laminated plates under thermal-mechanical loads. Eng Struct 2019;186: 345–355.

30. Kiani Y. Isogeometric large amplitude free vibration of graphene reinforced laminated plates in thermal environment using NURBS formulation. Comput Methods Appl Mech Eng 2018;332:86–101.

31. Fazzolari FA. Elastic buckling and vibration analysis of FG polymer composite plates embedding graphene nanoplatelet reinforcements in thermal environment, Mechanics of Advanced Materials and Structures 2019. DOI:10.1080/15376494.2019.1567886.

32. Thai CH, Ferreira AJM, Tran TD, Phung-Van P. Free vibration, buckling and bending analyses of multilayer functionally graded graphene nanoplatelets reinforced composite plates using the NURBS formulation. Compos Struct 2019;220:749-759.

33. Saidi AR, Bahaadini R, Majidi-Mozafari K. On vibration and stability analysis of porous plates reinforced by graphene platelets under aerodynamical loading. Compos Part B: Eng 2019;164:778-799.

34. Bekyarova E, Thostenson ET, Yu A, Kim H, Gao J, Tang J, Hahn HT, Chou T-W, Itkis ME, Haddon RC. Multiscale carbon nanotube-carbon fiber reinforcement for advanced epoxy composites. Langmuir 2007;23:3970–3974.

35. Papageorgiou DG, Li Z, Liu M, Kinloch IA, Young RJ. Mechanisms of mechanical reinforcement by graphene and carbon nanotubes in polymer nanocomposites. Nanoscale 2020;12:2228–2267.

36. Yang X, Wang Z, Xu M, Zhao R, Liu X. Dramatic mechanical and thermal increments of thermoplastic composites by multi-scale synergetic reinforcement: Carbon fiber and graphene nanoplatelets. Materials and Design 2013;44:74-80.

37. Hadden CM, Klimek-McDonald DR, Pineda EJ, King JA, Reichanadter AM, Miskioglu I, Gowtham S, Odegard GM. Mechanical properties of graphene, nanoplatelet/carbon fiber/epoxy hybrid composites: Multiscale modeling and experiments. Carbon 2015;95:100-112.

38. Aluko O, Gowtham S, Odegard GM. Multiscale modeling and analysis of graphene nanoplatelet/carbon fiber/epoxy hybrid composite. Compos Part B: Eng 2017;131:82-90.

39. Imran KA, Shivakumar KN, Graphene-modified carbon/epoxy nanocomposites: Electrical, thermal and mechanical properties. Journal of Composite Materials 2019;53(1):93-106.

40. Al Mahmud H, Radue MS, Chinkanjanarot S, Pisani WA, Gowtham S, Odegard GM. Multiscale modeling of carbon fiber-graphene nanoplatelet-epoxy hybrid composites using a reactive force field. Compos Part B: Eng 2019;172:628-635.

41. Rafiee M, Nitzsche F, Labrosse MR. Modeling and mechanical analysis of multiscale fiber-reinforced graphene composites: Nonlinear bending, thermal post-buckling and large amplitude. International Journal of Non-Linear Mechanics 2018;103:104-112.

42. Gholami R, Ansari R, Gholami Y. Numerical study on the nonlinear resonant dynamics of carbon nanotube/fiber/polymer multiscale laminated composite rectangular plates with various boundary conditions. Aerospace Science and Technology 2018;78:118-129.

43. Ebrahimi F, Dabbagh A. Vibration analysis of multi-scale hybrid nanocomposite plates based on a Halpin-Tsai homogenization model. Compos Part B: Eng 2019; 173:106955.

44. Radebe IS, Drosopoulos GA, Adali S. Buckling of non-uniformly distributed graphene and fibre reinforced multiscale angle-ply laminates. Meccanica 2019;54; 2263–2279.

45. An H, Chen S, Huang H. Maximization of fundamental frequency and buckling load for the optimal stacking sequence design of laminated composite structures. Proceedings of the Institution of Mechanical Engineers, Part L: Journal of Materials: Design and Applications 2018, 146442071876502.

46. Kayikci R, Sonmez FO. Design of composite laminates for optimum frequency response. Journal of Sound and Vibration 2012;331(8):1759-1776.

47. Apalak MK, Karaboga D, Akay B. The Artificial Bee Colony algorithm in layer optimization for the maximum fundamental frequency of symmetrical laminated composite plates, Engineering Optimization 2014;46:3:420-437.

48. Sadr MH, Ghashochi Bargh H. Optimization of laminated composite plates for maximum fundamental frequency using Elitist-Genetic algorithm and finite strip method. Journal of Global Optimization 2011;54(4):707–728.

49. Kamarian S, Shakeri M, Karimi B, Pourasghar A. Free vibration analysis and design optimization of nanocomposite-laminated beams using various higher order beam theories and imperialist competitive algorithm. Polymer Composites 2015;37(8):2442-2451.

50. Kamarian S, Shakeri M, Yas MH. Natural frequency analysis and optimal design of CNT/fiber/polymer hybrid composites plates using Mori-Tanaka approach, GDQ technique, and firefly algorithm. Polymer Composites 2016;39(5);1433–1446.

51. Reddy JN. Mechanics of Laminated Composite Plates and Shells. 2nd ed. CRC Press, 2004.

52. Higham NJ. Cholesky factorization. In: Padua D, (editor). Encyclopedia of Parallel Computing. Springer, 2011 Boston, MA.

53. MATLAB. (2016). version 9.0.0.341360 (R2016a). Natick, Massachusetts: The MathWorks Inc.

54. Gill PE, Murray W, Wright MH. Numerical Linear Algebra and Optimization. Addison Wesley, 1991.

55. Huang Y, Yang Z, Liu A, Fu J. Nonlinear buckling analysis of functionally graded graphene reinforced composite shallow arches with elastic rotational constraints under uniform radial load. Mater 2018;11(6):910.

56. Yang J, Chen D, Kitipornchai S. Buckling and free vibration analyses of functionally graded graphene reinforced porous nanocomposite plates based on Chebyshev-Ritz method. Compos Struct 2018;193:281-294.

57. Chen D, Yang J, Kitipornchai S. Nonlinear vibration and postbuckling of functionally graded graphene reinforced porous nanocomposite beams. Compos Science Tech 2017;142:235-245.

58. Yang J, Wu H, Kitipornchai S. Buckling and postbuckling of functionally graded multilayer graphene platelet-reinforced composite beams. Compos Struct 2017;161:111-118.

59. Shen H-S. A comparison of buckling and postbuckling behavior of FGM plates with piezoelectric fiber reinforced composite actuators. Compos Struct 2009;91:375–384.

60. Song M, Yang J, Kitipornchai S, Zhu W. Buckling and postbuckling of biaxially compressed functionally graded multilayer graphene nanoplatelet-reinforced polymer composite plates. International Journal of Mechanical Sciences 2017;131-132:345-355.

61. Wang Y, Feng C, Zhao Z, Yang J. Eigenvalue buckling of functionally graded cylindrical shells reinforced with graphene platelets (GPL). Compos Struct 2018;202:38-46.

62. Wang Y, Feng C, Zhao Z, Yang J. Buckling of graphene platelet reinforced composite cylindrical shell with cutout. International Journal of Structural Stability and Dynamics 2018;18(03):1850040:1-17.

63. Nocedal J, Wright. SJ. Numerical Optimization. Springer Series in Operations Research and Financial Engineering, Springer, 2006.

64. Zabinsky ZB. Optimal design of composite structures. In: Floudas CA, Pardalos PM, editors. Encyclopedia of Optimization. Kluwer Academic Publishers, 2001. p. 153-160.

65. Papalambros PY, Wilde DJ. Principles of Optimal Design, Modeling and Computation, Cambridge University Press, 2017.

66. Song M, Kitipornchai S, Yang J. Free and forced vibrations of functionally graded polymer composite plates reinforced with graphene nanoplatelets. Compos Struct 2017;159:579-588.

67. Kanaun SK, Jeulin D. Elastic properties of hybrid composites by the effective field approach, J Mech Phy Solids 2001;49:2339-2367.

68. Genin GM, Birman V. Micromechanics and structural response of functionally graded, particulate-matrix, fiber-reinforced composites. Int J Solids Struct 2009;46(10):2136-2150.

Appendix

1. Strain energy

The strain energy of the laminated composite plate is expressed as

$$U = \frac{1}{2}\int_{V_e}\left(\{\varepsilon_{b0}\}^T\left[\overline{Q_b}\right]\{\varepsilon_{b0}\} + \{\varepsilon_{b0}\}^T z[\overline{Q_b}]\{\kappa\} + \{\kappa\}^T z\left[\overline{Q_b}\right]\{\varepsilon_{b0}\} + \{\kappa\}^T z^2\left[\overline{Q_b}\right]\{\kappa\} + \{\varepsilon_{s0}\}^T[\overline{Q_s}]\{\varepsilon_{s0}\}\right)dV$$

$$= \frac{1}{2}\int_{V_e}\begin{Bmatrix}\{\varepsilon_{b0}\}\\ \{\kappa\}\\ \{\varepsilon_{s0}\}\end{Bmatrix}^T\begin{bmatrix}[\overline{Q_b}] & z[\overline{Q_b}] & 0\\ z[\overline{Q_b}] & z^2[\overline{Q_b}] & 0\\ 0 & 0 & \left[\overline{Q_s}\right]\end{bmatrix}\begin{Bmatrix}\{\varepsilon_{b0}\}\\ \{\kappa\}\\ \{\varepsilon_{s0}\}\end{Bmatrix}dV = \frac{1}{2}\int_{V_e}\{\overline{\varepsilon}\}^T[C(z)]\{\overline{\varepsilon}\}dV \quad \text{(A1)}$$

where V_e is the volume of an element. Substituting for $\{\varepsilon_{b0}\}$, $\{\kappa\}$ and $\{\varepsilon_{s0}\}$ in the above equation, U can be written as

$$U = \frac{1}{2}\{d\}_e{}^T[K]_e\{d\}_e \quad \text{(A2)}$$

where

$$[K]_e = \sum_{k=1}^{N}\left[\int_{V_k}[B]^T[C(z)]_k[B]dV_k\right] \quad \text{(A3)}$$

In equation (A3) V_k is the volume of the k^{th} layer, N is the number of lamina, $[C]$ is the elasticity tensor and $[B]$ is the strain – displacement matrix.

2. Kinetic energy

The kinetic energy of the composite plate is expressed as

$$T = \frac{1}{2}\sum_{k=1}^{N}\left(\int_{V_k}\rho_k\left[\{\dot{u_1}\}^2 + \{\dot{u_2}\}^2 + \{\dot{u_3}\}^2\right]dV_k\right), \quad \text{(A4)}$$

where ρ_k is the density of the k^{th} layer. Substituting the displacements relations of Eq. (1), Eq. (A4) becomes

$$T = \frac{1}{2}\sum_{k=1}^{N}\left(\int_{V_k}\rho_k\left[\dot{u}^2 + 2z\dot{u}\dot{\varphi}_x + \dot{v}^2 + 2z\dot{v}\dot{\varphi}_y + \dot{w}^2 + z^2\dot{\varphi}^2 + z^2\dot{\varphi}_y^2\right]dV_k\right)$$

$$= \frac{1}{2}\sum_{k=1}^{N}\int_{V_k}\begin{Bmatrix} u \\ v \\ w \\ \varphi_x \\ \varphi_y \end{Bmatrix}^T \rho_k \begin{bmatrix} 1 & 0 & 0 & -z & 0 \\ 0 & 1 & 0 & 0 & -z \\ 0 & 0 & 1 & 0 & 0 \\ -z & 0 & 0 & z^2 & 0 \\ 0 & -z & 0 & 0 & z^2 \end{bmatrix}\begin{Bmatrix} u \\ v \\ w \\ \varphi_x \\ \varphi_y \end{Bmatrix} dV_k = \sum_{k=1}^{N}\frac{1}{2}\int_{V_k}\left\{\dot{\overline{u}}\right\}^T[I(z)]_k\{\dot{\overline{u}}\}dV_k \qquad \text{(A5)}$$

Equation (A5) then becomes:

$$T = \frac{1}{2}\{\dot{d}\}^T[M]\{\dot{d}\} \qquad \text{(A6)}$$

where

$$[M]_e = \int_{A_e}\sum_{k=1}^{N}\int_{z_{k-1}}^{z_k}[N]^T[I(z)]_k[N]dzdA \qquad \text{(A7)}$$

where A_e is the area of the element and z_{k-1}, z_k are the *z* coordinates of the laminate corresponding to the bottom and top surface of the *k*th layer.

3. Work done by the mechanical forces

The work done by the mechanical forces is given by

$$W = \{\overline{u}\}^T\{f_c\} + \int_{S_1}\{\overline{u}\}^T\{f_s^{(i)}\}dS + \int_V\{\overline{u}\}^T\{f_v\}dV$$

$$= \{d\}_e{}^T[N]^T\{f_c\} + \{d\}_e{}^T\int_{S_1}[N]^T\{f_s^{(i)}\}dS + \{d\}_e{}^T\int_V[N]^T\{f_v\}dV \equiv \{d\}_e{}^T\{F_m\}_e \qquad \text{(A8)}$$

In Equation (A8), $\{f_c\}$ denotes the concentrated forces and $\{f_s\}$, $\{f_v\}$ denote the surface and volume forces, respectively. S_1 is the surface area, V is the volume and $\{F_m\}_e$ is the vector of the applied mechanical forces on an element.